Nine-Coordinate Lanthanide Podates with Predetermined Structural and Electronic Properties: Facial Organization of Unsymmetrical Tridentate Binding Units by a Protonated Covalent Tripod

Fabien Renaud,[†] Claude Piguet,*[,†] Gérald Bernardinelli,[§] Jean-Claude G. Bünzli,[‡] and Gérard Hopfgartner[⊥]

Contribution from the Department of Inorganic, Analytical and Applied Chemistry and the Laboratory of X-ray Crystallography, University of Geneva, CH-1211 Geneva 4, Switzerland, the Institute of Inorganic and Analytical Chemistry, University of Lausanne, CH-1015 Lausanne, Switzerland, and the Pharmaceuticals Division, F. Hoffmann-La Roche Ltd, CH-4070 Basle, Switzerland

Received March 19, 1999

Abstract: Three unsymmetrical tridentate pyridine-2,6-dicarboxamide binding units have been connected to the tris(2-(*N*-methyl)aminoethyl)amine tripod to give the podand L^{10} that exists as a statistical mixture of four conformers in solution. In aqueous acidic medium, the protonated apical nitrogen atom of the tripod (pK_a-($[L^{10}+H]^+$) = 4.66(2)) adopts an endo conformation compatible with the formation of bi- and trifurcated hydrogen bonds with the oxygen atoms of the proximal carboxamide groups, thus producing a clipped conformation preorganized for the complexation of lanthanide metal ions. Reactions of L^{10} and $[L^{10}+H]^+$ with $Ln(ClO_4)_3$ (Ln = La−Lu) in acetonitrile provide stable nine-coordinate podates $[Ln(L^{10})]^{3+}$ and $[Ln(L^{10}+H)]^{4+}$. Thermodynamic investigations indicate that the increased electrostatic repulsion associated with the complexation of the protonated podand is compensated by preorganization leading to only minor effects on the stability of the final podates. A structural characterization in solution using paramagnetic NMR concludes that a weak interaction between Ln(III) and the lone pair of the apical nitrogen atom of the tripod in $[Ln(L^{10})]^{3+}$ is removed in $[Ln(L^{10}+H)]^{4+}$ leading to a distortion of the coordination site. The crystal structure of the complex $[Eu(L^{10}+H)](CF_3SO_3)_3(PF_6)(CH_3CN)_{0.5}$ (**12**, $EuC_{46}H_{62.5}N_{10.5}O_{15}F_{15}PS_3$, trigonal, $R\bar{3}$, $Z = 6$) reveals a cationic conical triple-helical podate $[Eu(L^{10}+H)]^{4+}$ resulting from the wrapping of the three meridionally tricoordinated chelating units about the metal ion. A remarkable trifurcated hydrogen bond ($N-H\cdots(O=C)_3$) rigidifies the tripod and forces Eu(III) to lie at the center of the pseudo-tricapped trigonal prismatic cavity. High-resolution emission spectroscopy demonstrates that Eu(III) is efficiently protected within the podate whose resistance toward hydrolysis is significantly improved compared to related nonclipped triple-helical complexes. The implications of covalent tripod for the design of nine-coordinate lanthanide building blocks with predetermined structural, thermodynamic, and electronic properties is discussed.

Introduction

It has been realized recently that lanthanide complexes possessing a high degree of structural organization associated with tunable electronic and magnetic properties are promising precursors for molecular and supramolecular devices[1] working as (i) luminescent probes for time-resolved fluoroimunoassays[2] and signaling and labeling technologies,[3] (ii) contrast agents for magnetic resonance imaging,[4] (iii) magnetic probes in liquid crystals,[5] and (iv) catalysts for RNA and DNA hydrolysis.[6] As a result of the poor stereochemical preferences and variable coordination numbers of lanthanide(III) metal ions,[7] Ln(III), the structural control of the final architectures essentially arises from weak but crucial interactions between the wrapped ligand strands according to the *induced fit* concept.[1] In this context, semirigid

[†] Department of Inorganic, Analytical and Applied Chemistry, 30 quai E. Ansermet, CH-1211-Geneva 4. E-mail: Claude.Piguet@chiam.unige.ch.
[§] Laboratory of X-ray Crystallography, 24 quai E. Ansermet, CH-1211-Geneva 4.
[‡] Institute of Inorganic and Analytical Chemistry, BCH 1402, CH-1015 Lausanne.
[⊥] Pharmaceuticals Division, F. Hoffmann-La Roche Ltd, PRNS 68/142, CH-4070 Basle.

(1) (a) Piguet, C.; Bünzli, J.-C. G. *Chimia* **1998**, *52*, 579. (b) Parker, D.; Senanayake, P. K.; Williams, J. A. G. *J. Chem. Soc., Perkin Trans. 2* **1998**, 2129. (c) Aime, S.; Batsanov, A. S.; Botta, M.; Dickins, R. S.; Faulkner, S.; Foster, C. E.; Harrisson, A.; Howard, J. A. K.; Moloney, J. M.; Norman, T. J.; Parker, D. A.; Royle, L.; Williams, J. A. G. *J. Chem. Soc., Dalton Trans.* **1997**, 3623.

(2) (a) Hemmilä, I.; Stahlberg, T.; Mottram, P. *Bioanalytical Applications of Labeling Technologies*, 2nd ed.; Wallac Oy: Turku, 1995. (b) Mathis, G. *Clin. Chem.* **1995**, *41*, 1391.

(3) (a) De Silva, A. P.; Gunaratne, H. Q. N.; Gunnlaugsson, T.; Huxley, A. J. M.; McCoy, C. P.; Rademacher, J. T.; Rice, T. E. *Chem. Rev.* **1997**, *97*, 1515. (b) Sueda, S.; Ihara, T.; Juskowiak, B.; Takagi, M. *Anal. Chim. Acta* **1998**, *365*, 27.

(4) (a) Lauffer, R. B. In *MRI Clinical Magnetic Resonance Imaging*, 2nd ed.; Edelman, R. E., Zlatkin, M. B., Hesselink, J. R., Eds; W. B. Saunders Co.: Philadelphia, 1996; Vol. 1, Chapter 5. (b) Aime, S.; Botta, M.; Fasano, M.; Terreno, E. *Chem. Soc. Rev.* **1998**, *27*, 19.

(5) (a) Galyametdinov, Y.; Athanassopoulou, A. M.; Kharitonova, O.; Soto-Bustamante, E. A.; Ovchinnikov, I. K.; Hasse, W. *Chem. Mater.* **1996**, *8*, 922. (b) Bikhantaev, I.; Galyametdinov, Y.; Kharitonova, O.; Ovchinnikov, I. K.; Bruce, D. W.; Dunmur, D. A.; Guillon, D.; Heinrich, B. *Liq. Cryst.* **1996**, *20*, 489. (c) Binnemans, K.; Van Deun, R.; Bruce, D. W.; Galyametdinov, Y. G. *Chem. Phys. Lett* **1999**, *300*, 509.

(6) (a) Bruice, T. C.; Tsubouchi, A.; Dempey, R. O.; Olson, L. P. *J. Am. Chem. Soc.* **1996**, *118*, 9867. (b) Oh, S. J.; Choi, Y.-S.; Hwangbo, S.; Bae, S. C.; Ku, J. K.; Park, J. W. *Chem. Commun.* **1998**, 2189. (c) Häner, R.; Hall, J. *Antisense Nucleic Acid Drug Develop.* **1997**, *7*, 423.

(7) Choppin, G. R. In *Lanthanide Probes in Life, Chemical and Earth Sciences*; Bünzli, J.-C. G., Choppin, G. R., Eds.; Elsevier Publishing Co: Amsterdam, 1989; Chapter 1.

10.1021/ja990898w CCC: $18.00
Published on Web 09/23/1999

symmetrical tridentate binding units containing a central pyridine ring L^{1-4} have been shown to produce nine-coordinate pseudo-tricapped trigonal prismatic sites in $[Ln(L^1\text{-}2H)_3]^{3-}$ [8] and $[Ln(L^i)_3]^{3+}$ [9-11] ($i = 2-4$) with tunable structural, geometrical, and thermodynamic properties. An improved control of the electronic properties requires the development of unsymmetrical tridentate units possessing two different sidearms connected to the 2- and 6-positions of the central pyridine ring as demonstrated by the facial C_3-symmetrical building block $[Eu(L^5)_3]^{3+}$ found in heterobimetallic helicates[12] which exhibits an emission quantum yield increased by factors 20 and 2000 compared to those measured for the related D_3-symmetrical complexes $[Eu(L^3)_3]^{3+}$ [9] and $[Eu(L^4)_3]^{3+}$.[13] However, the controlled facial arrangement of three unsymmetrical tridentate binding units around Ln(III) implies their connection to a tripod which prevents isomerization with the statistically favored C_1-symmetrical meridional isomer.[1] Facial pseudo-octahedral d-block complexes have been extensively used as noncovalent tripods to organize facial nonadentate coordination sites in self-assembled heterobimetallic d−f triple-stranded helicates (HHH)-$[LnM(L^6)_3]^{5+}$ (Ln = La−Lu; M = Fe, Co, Zn),[12] but covalent tripods which are systematically used for the facial organization of unsymmetrical bidentate binding units around six-coordinate d- or f-block metal ions[14] rarely have been involved in the related arrangement of tridentate binding units about nine-coordinate f-block ions.[15-17] Molecular models suggest that a regular wrapping of three bent and semirigid tricoordinated chelating units around a spherical ion induces severe structural requirements and this statement is supported by the observation that the potentially tridentate chelating sidearms of L^7 and L^8 are only dicoordinate to the same metal in the podates $[Ln(L^7\text{-}3H)(DMF)]_2$[15] and $[Ln(L^8\text{-}3H)(OH_2)_2]$[16] while L^9 provides an unsymmetrical terminal nine-coordinate site around Y(III) involving three phenolate oxygen atoms and six ether oxygen atoms of the hemiacetal groups.[17] Nevertheless, the introduction of a covalent tripod is expected (i) to improve the kinetic inertness[18] and the thermodynamic stability[19] of the final complexes which are crucial points for the development of lanthanide probes in aqueous media and (ii) to allow a precise structural control compatible with the design of extended directional and organized polymetallic edifices as previously demonstrated for d-block ions.[20] An elegant approach developed by Orvig and co-workers[21] uses podand-type ligands made of three bidentate binding units connected to short covalent tripods to achieve a fine structural and thermodynamic control of the final lanthanide complexes resulting from subtle noncovalent interstrand interactions (i.e., hydrogen bonds and hydrophobic effects). An unprecedent selectivity for the complexation of small Ln(III) in 1:2 complexes $[LnL_2]$ has been attributed to specific entropic effects which are relevant for explaining the preferred formation of 12-coordinate lanthanide capsules with related hexadentate podands.[22] A careful consideration of the crystal structure of the pseudo-D_3 triple-helical complexes $[Ln(L^3)_3]^{3+}$ (Ln = La, Eu)[9] suggests that the endo conformation of a tris(2-aminoethyl)amine (TREN) tripod would be suitable for capping one trigonal face of the prism in the complexes without inducing too severe steric constraints, thus leading to a podate in which Ln(III) would be nine-coordinate by three unsymmetrical tridentate binding units. Here we report the preparation and complexation properties of the new podand L^{10} that is designed to encapsulate nine-coordinate tricapped trigonal prismatic lanthanide ions. The nature and geometry of the coordination sphere have been carefully investigated in the solid state and in solution to detect structural and electronic changes associated with the introduction of the covalent tripod. The protonation of the apical nitrogen atoms plays a crucial role in the organization and rigidification of the final architecture which has been assigned to the formation of a trifurcated hydrogen bond within the covalent tripod. A partial report of this work appeared as a preliminary communication.[23]

Results

Synthesis and Structure of the Podand L^{10} in Solution. The attachment of chelating sidearms to the tris(2-aminoethyl)-amine (TREN) tripod via secondary amide groups has been shown to provide a network of intramolecular OC−N−H···N-(apical) hydrogen bonds which severely constraints the covalent tripod.[14] (i) To allow sufficient flexibility within the TREN tripod to facially organize semirigid bent tridentate binding units around nine-coordinate metal ions and (ii) to limit the quenching of luminescent Ln(III) (Ln = Eu, Tb) by high-frequency N−H oscillators in the final podate,[24] we have introduced unsymmetrical tertiary amide connectors in L^{10} which remove NH hydrogen donors. A selective trialkylation of TREN gives tris(2-(*N*-methylamino)ethyl)amine (Me-TREN, **2**) in two steps[25] which is reacted with an excess of the acyl chloride derivative of the tridentate synthon **3**[12a] to produce the target ligand L^{10} in good yield (86%, Scheme 1). As a result of

(8) (a) Grenthe, I. *J. Am. Chem. Soc.* **1961**, *83*, 360. (b) Brayshaw, P. A.; Bünzli, J.-C. G.; Froidevaux, P.; Harrowfield, J. M.; Kim, Y.; Sobolev, A. N. *Inorg. Chem.* **1995**, *34*, 2068. (c) Harrowfield, J. M.; Kim, Y.; Skelton, B. W.; White, A. H. *Aust. J. Chem.* **1995**, *48*, 807 and references therein.

(9) Renaud, F.; Piguet, C.; Bernardinelli, G.; Bünzli, J.-C. G.; Hopfgartner, G. *Chem. Eur. J.* **1997**, *3*, 1646.

(10) Renaud, F.; Piguet, C.; Bernardinelli, G.; Bünzli, J.-C. G.; Hopfgartner, G. *Chem. Eur. J.* **1997**, *3*, 1660.

(11) Petoud, S.; Bünzli, J.-C. G.; Renaud, F.; Piguet, C.; Schenk, K. J.; Hopfgartner, G. *Inorg. Chem.* **1997**, *36*, 5750.

(12) (a) Piguet, C.; Bünzli, J.-C. G.; Bernardinelli, G.; Hopfgartner, G.; Petoud, S.; Schaad, O. *J. Am. Chem. Soc.* **1996**, *118*, 6681. (b) Piguet, C.; Rivara-Minten, E.; Bernardinelli, G.; Bünzli, J.-C. G.; Hopfgartner, G. *J. Chem. Soc., Dalton Trans.* **1997**, 421. (c) Rigault, S.; Piguet, C.; Bernardinelli, G.; Hopfgartner, G. *Angew. Chem., Int. Ed. Engl.* **1998**, *37*, 169.

(13) Piguet, C.; Bünzli, J.-C. G.; Bernardinelli, G.; Bochet, C. G.; Froidevaux, P. *J. Chem. Soc., Dalton Trans.* **1995**, 83.

(14) (a) Wainwright, K. P. *Coord. Chem. Rev.* **1997**, *166*, 35. (b) Weizman, H.; Libman, J.; Shanzer, A. *J. Am. Chem. Soc.* **1998**, *120*, 2188. (c) Jäntti, A.; Wagner, M.; Suontamo, R.; Kolehmainen, E.; Rissanen, K. *Eur. J. Inorg. Chem.* **1998**, 1555. (d) Serratrice, G.; Boukhalfa, H.; Beguin, C.; Baret, P.; Caris, C.; Pierre, J.-L. *Inorg. Chem.* **1997**, *36*, 3898. (e) Ng, C. Y.; Rodgers, S. J.; Raymond, K. N. *Inorg. Chem.* **1989**, *28*, 2062. (f) Wietzke, R.; Mazzanti, M.; Latour, J.-M.; Pécaut, J. *J. Chem. Soc., Dalton Trans*, **1998**, 4087. (g) Balzani, V.; Berghmans, E.; Lehn, J.-M.; Sabbatini, N.; Terörde, R.; Ziessel, R. *Helv. Chim. Acta* **1990**, *73*, 1149.

(15) Xu, J.; Franklin, S. J.; Whisenhunt, D. W.; Raymond, K. N. *J. Am. Chem. Soc.* **1995**, *17*, 7245.

(16) Brianese, N.; Casellato, U.; Tamburini, S.; Tomasin, P.; Vigato, P. A. *Inorg. Chim. Acta* **1998**, *272*, 235.

(17) Archibald, S. J.; Blake, A. J.; Parsons, S.; Schröder, M.; Winpenny, R. E. P. *J. Chem. Soc., Dalton Trans.* **1997**, 173.

(18) Josceanu, A. M.; Moore, P. *J. Chem. Soc., Dalton Trans.* **1998**, 369.

(19) Motekaitis, R. J.; Martell, A. E.; Handcock, R. A. *Coord. Chem. Rev.* **1994**, *133*, 39.

(20) (a) Blanc, S.; Yakirevich, P.; Leize, E.; Meyer, M.; Libman, J.; Van Dorsselaer, A.; Albrecht-Gary, A.-M.; Shanzer, A. *J. Am. Chem. Soc.* **1997**, *119*, 4934. (b) Libman, J.; Tor, Y.; Shanzer, A. *J. Am. Chem. Soc.* **1987**, *109*, 5880.

(21) (a) Caravan, P.; Hedlund, T.; Liu, S.; Sjöberg, S.; Orvig, C. *J. Am. Chem. Soc.* **1995**, *117*, 11230. (b) Lowe, M. P.; Caravan, P.; Rettig, S. J.; Orvig, C. *Inorg. Chem.* **1998**, *37*, 1637.

(22) Jones, P. L.; Amoroso, A. J.; Jeffery, J. C.; McCleverty, J. A.; Psillakis, E.; Rees, L. H.; Ward, M. D. *Inorg. Chem.* **1997**, *36*, 10 and references therein.

(23) Renaud, F.; Piguet, C.; Bernardinelli, G.; Hopfgartner; G.; Bünzli, J.-C. G. *Chem. Commun.* **1999**, 457.

(24) Choppin, G. R.; Peterman, D. R. *Coord. Chem. Rev.* **1998**, *174*, 283.

(25) Schmidt, H.; Lensink, C.; Xi, S. K.; Verkade, J. G. *Z. Anorg. Allg. Chem.* **1989**, *578*, 75.

Chart 1

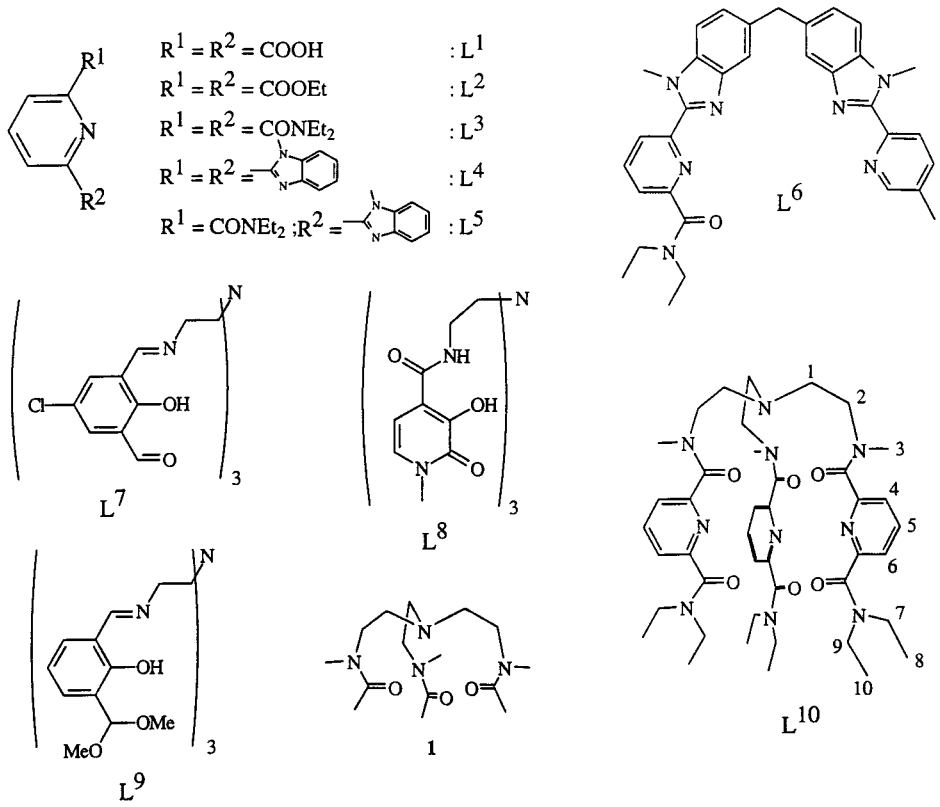

hindered rotations at room temperature about the C−N bonds of the three unsymmetrical tertiary amide connectors, we expect the formation of a mixture of four conformers which are dynamically inert on the NMR time scale and characterized by cis or trans orientations of the methyl groups C^3 with respect to the oxygen atom of the carboxamide: cis−cis−cis (CCC, C_{3v} symmetry), cis−cis−trans (CCT, C_s), cis−trans−trans (CTT, C_s), and trans−trans−trans (TTT, C_{3v}). (According to IUPAC nomenclature, the cis orientation described in the text corresponds to the *E* isomer when we consider a double bond between the nitrogen and the carbon atoms of the amide group. Consequently, the trans orientation is related to the *Z* isomer.) Six singlets are observed for the protons of the methyl groups C^3 in the ^{1}H-NMR spectrum of L^{10} in CD_3CN (298 K: 2.72, 2.82, 2.85, 2.95, 2.97, and 3.08 ppm) with relative intensity of 1:1:2:2:1:1 corresponding to the statistical distribution: CCC (12.5%) and TTT (12.5%) give two singlets of intensity 1 and CCT (37.5%) and CTT (37.5%) provide four signals, two with intensities of 2 and two with intensities of 1 (Figure 1a). According to the complexity of the ^{1}H-NMR signals in the aliphatic region (we expect 12 quartets and 12 triplets in the range 2.8−3.4 ppm corresponding to the protons $H^{1,1'}$, $H^{2,2'}$, $H^{7,7'}$, and $H^{9,9'}$), we were not able to assign the observed signals for the protons of the methyl groups C^3 to each complex by using intramolecular NOE effects. Heating the solution to 343 K (CD_3CN) produces a broadening of the signals, but coalescence is only obtained at 413 K in DMSO-d_6 leading to the expected dynamically averaged C_{3v}-symmetrical structure for L^{10} on the NMR time scale (Table 1). The addition of 1 equiv of trifluoromethanesulfonic acid (TfOH ≡ CF_3SO_3H) in these conditions induces downfield shifts for $H^{1,1'}$ and $H^{2,2'}$ ($\Delta\delta(H^{1,1'}) = 0.85$ ppm, $\Delta\delta(H^{2,2'}) = 0.44$ ppm) which are characteristic for the protonation of the apical nitrogen atom in the Me-TREN tripod.[26] The minor variation of the signal of H^5 ($\Delta\delta(H^5) =$ 0.05 ppm) excludes the protonation of the pyridine ring.[27] When the titration of L^{10} by TfOH is monitored by ^{1}H-NMR in CD_3CN at 298 K, a striking simplification of the spectrum is evidenced after the addition of 1 equiv of acid. The blocked methyl groups C^3 of $[L^{10}+H]^+$ give only three singlets at lower fields compared to L^{10} (3.01, 3.08, and 3.14 ppm) with relative intensities of 1:3:2, respectively (Figure 1b). Two-dimensional {^{1}H−^{1}H}-NMR correlation spectroscopy and NOE measurements demonstrate the almost exclusive existence of two conformers in the mixture: 50% of a C_{3v}-symmetrical species (CCC or TTT) associated with the singlet at 3.08 ppm and 50% of a C_s-symmetrical species (CTT or TCC; singlets at 3.01 and 3.14 ppm). Traces of the two remaining conformers can be detected in the spectrum and correspond to less than 2% of the mixture and have been neglected. Potentiometric titrations of L^{10} with TfOH in acetonitrile/water mixtures definitively establish the fixation of a single proton in the pH range 8.0−1.0 with $pK_a([L^{10}+H]^+) = 4.66(2)$ (H_2O/CH_3CN = 95:5, 0.1 M $NaClO_4$) and $pK_a([L^{10}+H]^+) = 4.3(2)$ (H_2O/CH_3CN = 5:95, 0.1 M NBu_4ClO_4). Similar values are found for the model compound **1** ($pK_a([\mathbf{1}+H]^+) = 5.19(2)$ (H_2O/CH_3CN = 95:5, 0.1 M $NaClO_4$) and $pK_a([\mathbf{1}+H]^+) = 5.3(2)$ (H_2O/CH_3CN = 5:95, 0.1 M NBu_4ClO_4)) that does not possess pyridine rings, thus confirming the protonation of the apical nitrogen atom of the Me-TREN tripod in L^{10}. Surprisingly, $pK_a([L^{10}+H]^+)$ and $pK_a([\mathbf{1}+H]^+)$ are approximately 6 orders of magnitude lower than that of the triethylammonium cation (pK_a = 11.01), but recent results based on protonated cryptands[28] and tris(2-hydroxyethyl)amine podands[29] suggest that the protonated apical nitrogen adopts an endo conformation stabilized by intramolecular hydrogen bonds with the surrounding oxygen atoms of the sidearms. The hydrophilicity of the resulting clipped

(26) Caravan, P.; Orvig, C. *Inorg. Chem.* **1997**, *36*, 236.

(27) Lavallee, D. K.; Baughman, M. D.; Phillips, M. P. *J. Am. Chem. Soc.* **1977**, *99*, 718.

(28) MacGillivray, L. R.; Atwood, J. L. *J. Org. Chem.* **1995**, *60*, 4972.

(29) Castellari, C.; Ottani, S. *Acta Crystallogr.* **1996**, *C52*, 2619.

Scheme 1[a]

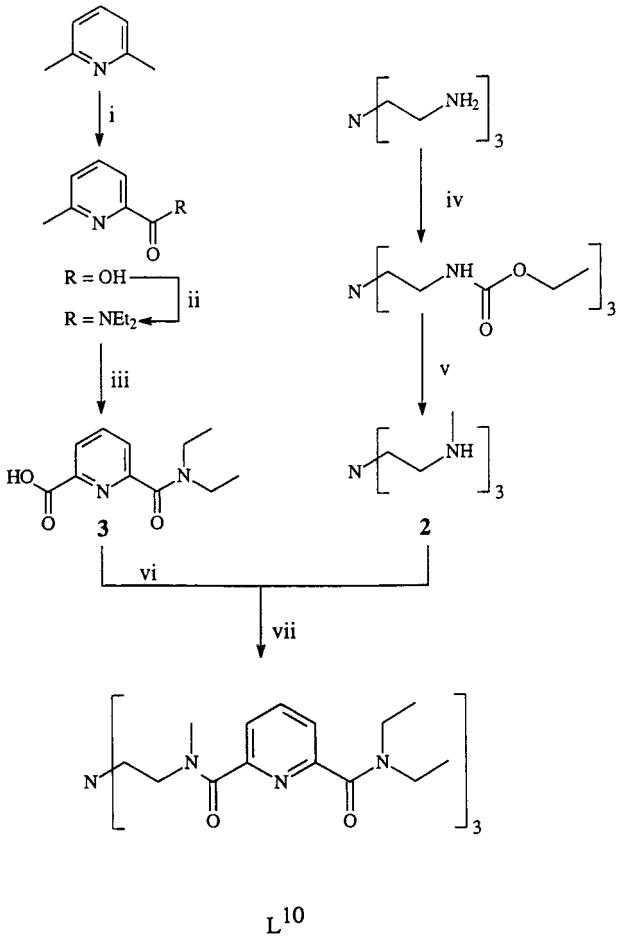

[a] Reagents: (i) $KMnO_4$, H_2O; (ii) (1) $SOCl_2$, CH_2Cl_2, $DMF_{cat.}$; (2) Et_2NH, CH_2Cl_2; (iii) SeO_2, pyridine; (iv) $ClCO_2Et$, KOH, $C_6H_6-H_2O$; (v) $LiAlH_4$, THF; (vi) $SOCl_2$, CH_2Cl_2, $DMF_{cat.}$; (vii) Et_3N, CH_2Cl_2.

conformation is severely reduced leading to a drastic destabilization of the protonated form in polar media. These observations together with the NMR data strongly suggest that protonation of the apical nitrogen atom results in the formation of a clipped conformation stabilized by bifurcated (TTC, C_s) or trifurcated (TTT, C_{3v}) hydrogen bonds between the acidic proton and the oxygen atoms of the proximal trans tertiary amide groups (Scheme 2).[30]

Formation of the Podates $[Ln(L^{10})]^{3+}$ (Ln = La−Lu) in Solution. Spectrophotometric titrations of L^{10} in acetonitrile (10^{-4} m) with $Ln(ClO_4)_3 \cdot xH_2O$ (Ln = La−Lu, $x = 6-8$) display a sharp end point for $Ln:L^{10} = 1.0$ in agreement with the formation of the podate $[Ln(L^{10})]^{3+}$ (Figure 2). Factor analyses involve the exclusive formation of the 1:1 complex for Ln = Nd−Lu (Figure 2b), while a second absorbing complex is evidenced for Ln = La−Pr (Figure 2a). The spectrophotometric data can be satisfactorily fitted with a nonlinear least-squares technique[31] to eq 1 (Ln = Nd−Lu) and to eqs 1 and 2 (Ln = La−Pr) with stability constants $\log(\beta_{ijk}^{Ln})$ given in Table 2.

$$Ln^{3+} + L^{10} \rightleftharpoons [LnL^{10}]^{3+} \quad \log(\beta_{110}^{Ln}) \qquad (1)$$

$$Ln^{3+} + 2\,L^{10} \rightleftharpoons [Ln(L^{10})_2]^{3+} \quad \log(\beta_{120}^{Ln}) \qquad (2)$$

The β_{110}^{Ln} values do not reflect a clear size-discriminating effect

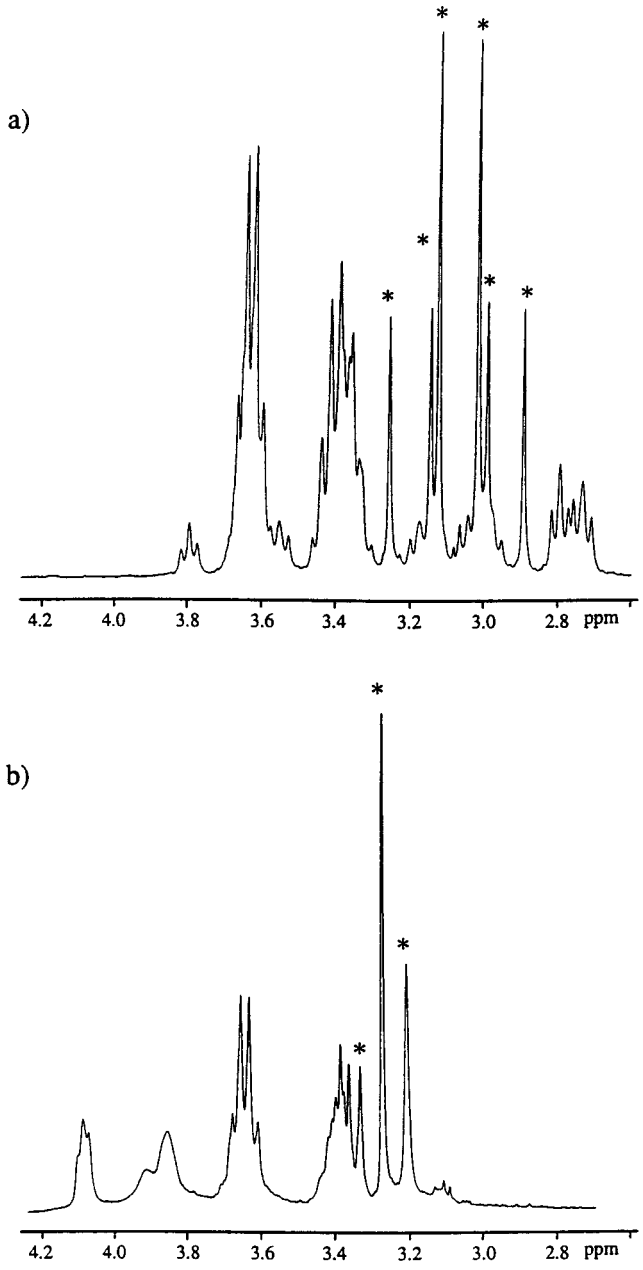

Figure 1. Part of the 300 MHz ^{1}H-NMR spectra of (a) L^{10} and (b) $[L^{10}+H]^+$ in CD_3CN at 298 K. The singlet resonances of the C^3 methyl protons are indicated with an asterisk.

along the lanthanide series, except for a minor increase of the stability for the light Ln(III) ions which strongly contrasts with the classical electrostatic trend (i.e. the increase of the stability constants with decreasing ionic radius)[7,8a,21] previously observed for the related nonclipped triple-helical complexes $[Ln(L^3)_3]^{3+}$ in the same conditions.[9] Steric constraints associated with the covalent Me-TREN tripod in $[Ln(L^{10})]^{3+}$ may explain the reduced affinity for smaller Ln(III) ions which induce a tighter helical wrapping of the ligand strands,[9] but specific solvation effects in acetonitrile have to be considered (see Discussion). The formation of 1:2 complexes $[Ln(L^{10})_2]^{3+}$ is limited to large Ln(III) ions and is confirmed by ES-MS titrations performed in the same conditions. Strong peaks assigned to $[Ln(L^{10})_2]^{3+}$ and $[Ln(L^{10})_2(ClO_4)]^{2+}$ are observed for Ln = La−Pr in

(30) Taylor, R.; Kennard, O.; Versichel, W. *J. Am. Chem. Soc.* **1984**, *106*, 244.

(31) Gampp, H.; Maeder, M.; Meyer, C. J.; Zuberbühler, A. D. *Talanta* **1985**, *32*, 95.

Table 1. NMR Shifts (with Respect to TMS) for Ligand L^{10} and Its Complexes $[LnL^{10}]^{3+}$ in CD_3CN and $[Ln(L^{10}+H)]^{4+}$ in CD_3CN/CD_3NO_2 (1:1) at 298K

	^{1}H-NMR shifts									
	H^1, $H^{1'}$	H^2, $H^{2'}$	H^3	H^4	H^5	H^6	H^7, $H^{7'}$	H^8	H^9, $H^{9'}$	H^{10}
L^{10} [a]	2.78	3.40	2.96	7.54	7.95	7.54	3.41	1.13	3.40	1.13
$[L^{10}+H]^+$ [a]	3.53	3.84	3.07	7.64	8.00	7.58	3.39	1.13	3.39	1.13
$[LaL^{10}]^{3+}$	*b*	*b*	3.32	8.07	8.31	8.01	*b*	1.38	*b*	0.53
$[La(L^{10}+H)]^{4+}$	3.86	3.86	3.49	8.20	8.41	8.12	3.60	1.37	3.23	0.70
$[CeL^{10}]^{3+}$	*b*	*b*	3.42	8.00	8.62	8.00	*b*	1.41	*b*	0.52
$[Ce(L^{10}+H)]^{4+}$	*b*	*b*	3.68	5.88	7.23	7.08	2.70	1.45	*b*	1.54
$[PrL^{10}]^{3+}$	0.87/0.99	2.35/2.44	3.30	9.36	9.72	9.02	3.83	1.51	2.69	0.35
$[Pr(L^{10}+H)]^{4+}$	7.51/9.52	5.48/6.24	3.58	6.86	7.80	7.81	2.93	1.56	4.39/5.90	1.65
$[NdL^{10}]^{3+}$	3.71/4.95	2.66/2.95	3.65	8.48	8.78	8.70	3.51/3.70	1.50	3.27/4.02	0.73
$[Nd(L^{10}+H)]^{4+}$	5.69/8.88	6.58/7.89	3.63	6.92	7.51	7.99	3.01/3.17	1.61	4.28/6.01	1.82
$[SmL^{10}]^{3+}$	2.47/2.70	2.96/4.27	3.34	8.12	8.51	8.02	3.53/3.71	1.40	3.03/3.30	0.61
$[Sm(L^{10}+H)]^{4+}$	4.74/5.56	3.98/4.21	3.53	7.79	8.13	7.92	3.43/3.66	1.42	3.24/3.66	0.98
$[EuL^{10}]^{3+}$	3.15/5.20	2.83/3.41	3.09	6.71	7.22	6.32	3.53/3.65	1.32	3.35/3.53	0.62
$[Eu(L^{10}+H)]^{4+}$	2.01/2.70	1.84/2.70	3.69	7.98	8.48	7.18	3.78/4.12	1.18	1.67/2.41	−0.35
$[YL^{10}]^{3+}$	2.58/2.74	3.00/4.27	3.39	8.17	8.35	8.10	3.53/3.77	1.40	2.95/3.18	0.62
$[Y(L^{10}+H)]^{4+}$	3.64/3.98	3.68/4.77	3.55	8.26	8.45	8.19	3.50/3.83	1.39	2.88/3.08	0.69
$[YbL^{10}]^{3+}$	3.68/4.05	3.40/5.52	3.73	7.57	7.84	7.97	3.08/4.39	1.29	2.72/3.40	0.43
$[Yb(L^{10}+H)]^{4+}$	−3.41/−1.97	−3.58/0.13	3.65	12.32	11.28	10.09	3.98/5.48	0.76	−1.60/−0.11	−3.67
$[LuL^{10}]^{3+}$	2.62/2.73	2.98/4.25	3.41	8.19	8.36	8.12	3.54/3.79	1.31	2.92/3.14	0.62
$[Lu(L^{10}+H)]^{4+}$	3.71/3.97	3.64/4.78	3.58	8.28	8.46	8.21	3.50/3.87	1.39	2.83/3.02	0.70

	^{13}C-NMR shifts									
	C^1	C^2	C^3	C^4	C^5	C^6	C^7	C^8	C^9	C^{10}
$[LaL^{10}]^{3+}$	55.98	49.42	38.09	127.88	142.44	127.66	44.89	13.81	43.45	11.42
$[La(L^{10}+H)]^{4+}$	58.70	46.17	39.48	128.53	142.68	127.86	44.95	13.26	43.17	11.24
$[CeL^{10}]^{3+}$	56.05	50.54	38.73	132.31	141.42	132.26	45.84	13.94	44.84	11.73
$[Ce(L^{10}+H)]^{4+}$	64.48	50.97	40.45	128.22	138.54	129.13	45.56	13.06	44.94	12.20
$[PrL^{10}]^{3+}$	53.82	48.07	38.13	141.85	139.66	141.51	46.48	13.22	44.25	10.74
$[Pr(L^{10}+H)]^{4+}$	62.94	50.45	41.26	136.47	137.53	137.08	46.18	12.91	46.28	12.16
$[NdL^{10}]^{3+}$	56.88	50.44	38.67	144.68	137.02	144.61	45.46	13.16	46.99	11.32
$[Nd(L^{10}+H)]^{4+}$	63.87	51.02	41.68	140.28	135.88	141.41	46.74	12.89	46.82	12.39
$[SmL^{10}]^{3+}$	55.77	49.72	38.17	127.24	142.96	126.99	44.14	13.82	44.93	11.49
$[Sm(L^{10}+H)]^{4+}$	59.87	47.05	39.77	127.16	143.00	126.79	44.36	13.48	45.21	11.73
$[EuL^{10}]^{3+}$	55.68	50.17	37.56	94.48	154.02	95.21	43.34	15.48	41.70	12.39
$[Eu(L^{10}+H)]^{4+}$	56.42	43.20	37.12	101.13	155.54	98.4	42.17	14.9	41.74	11.14
$[YL^{10}]^{3+}$	56.08	50.16	38.23	128.23	142.68	127.96	45.20	13.89	44.70	11.61
$[Y(L^{10}+H)]^{4+}$	59.37	46.50	39.76	128.87	143.18	128.33	45.60	13.51	44.64	11.63
$[YbL^{10}]^{3+}$	58.05	51.35	38.35	122.21	144.50	122.86	44.75	14.34	44.68	11.99
$[Yb(L^{10}+H)]^{4+}$	50.80	40.54	38.59	131.95	150.77	128.47	45.32	13.71	38.94	7.97
$[LuL^{10}]^{3+}$	56.22	50.34	38.21	128.42	142.54	128.11	45.25	13.88	44.92	11.66
$[Lu(L^{10}+H)]^{4+}$	59.60	46.49	39.71	129.02	143.00	128.46	44.92	13.49	45.78	11.72

[a] In DMSO-d_6 at 440 K. [b] Too broad or too complicated overlaped signals to be unambiguously assigned.

agreement with the existence of a significant amount of 1:2 complexes in solution. These signals become weak for Ln = Nd and almost completely disappear for Ln = Lu (Table S10, Supporting Information). To the best of our knowledge, there is no precedent for similar complexes with nonadentate podands, but we notice that (i) $[Ln(L^3)_3]^{3+}$ has been shown to react with a supplementary ligand to give $[Ln(L^3)_4]^{3+}$ in acetonitrile[9] and (ii) 1:2 lanthanide complexes with two hexadentate podands coordinated to Ln(III) have been previously reported by Ward and co-workers.[22] We suspect that large Ln(III) are less efficiently protected by the wrapped tridentate chelating units in $[Ln(L^{10})]^{3+}$ thus allowing further interactions with additional ligands.

The addition of water into acetonitrile (5% v/v; 2.78 M) prevents the formation of 1:2 complexes and spectrophotometric titrations can be fitted to eq 1 for the complete lanthanide series (Table 2). This behavior is in line with the fixation of a second podand in $[Ln(L^{10})_2]^{3+}$ by weak electrostatic interactions which are severely reduced in more polar solvents as previously suggested for $[Ln(L^3)_4]^{3+}$.[9] To substantiate this hypothesis, L^{10} has been titrated with $La(ClO_4)_3 \cdot 6H_2O$ in acetonitrile containing 5% of MeOH, a cosolvent with a lower polarity and a weaker affinity for Ln(III) than water. As expected, the formation of the two successive complexes $[La(L^{10})]^{3+}$ and $[La(L^{10})_2]^{3+}$ is restored, but with formation constants ($\log(\beta^{La}_{110}) = 7.8(1)$; $\log(\beta^{La}_{120}) = 12.5(2)$) slightly lower than those found in pure acetonitrile.

Structures of the Podates $[Ln(L^{10})]^{3+}$ (Ln = La−Lu) in Solution. According to eqs 1 and 2 and their associated thermodynamic constants, we calculate that a 1:1 mixture of L^{10} and $Ln(ClO_4)_3$ (Ln = La−Lu) in acetonitrile produces quantitatively and exclusively the podates $[Ln(L^{10})]^{3+}$ for a total ligand concentration of 0.05 M, thus allowing its structural investigation by NMR spectroscopy in these conditions. ^{1}H- and ^{13}C-NMR spectra of the diamagnetic podates $[Ln(L^{10})]^{3+}$ (Ln = La, Y, Lu) in CD_3CN display a single set of three aromatic signals corresponding to H^{4-6} and C^{4-6} respectively and implying C_3 or C_{3v} symmetries. However, the pairs of methylene protons $H^{1,1'}$, $H^{2,2'}$, $H^{7,7'}$, and $H^{9,9'}$ are diastereotopic in the podates leading to ^{1}H-NMR spectra only compatible with a C_3-symmetrical helical arrangement of the wrapped strands.[9,12a] The observation of strong intramolecular NOE effects between H^3−H^4 and H^6−$H^{7,7'}$ is diagnostic for a cis−cis conformation[9] of the tridentate binding units in $[Ln(L^{10})]^{3+}$ (i.e. the oxygen atoms of the carbonyl groups are cis to the nitrogen atom of the

Scheme 2

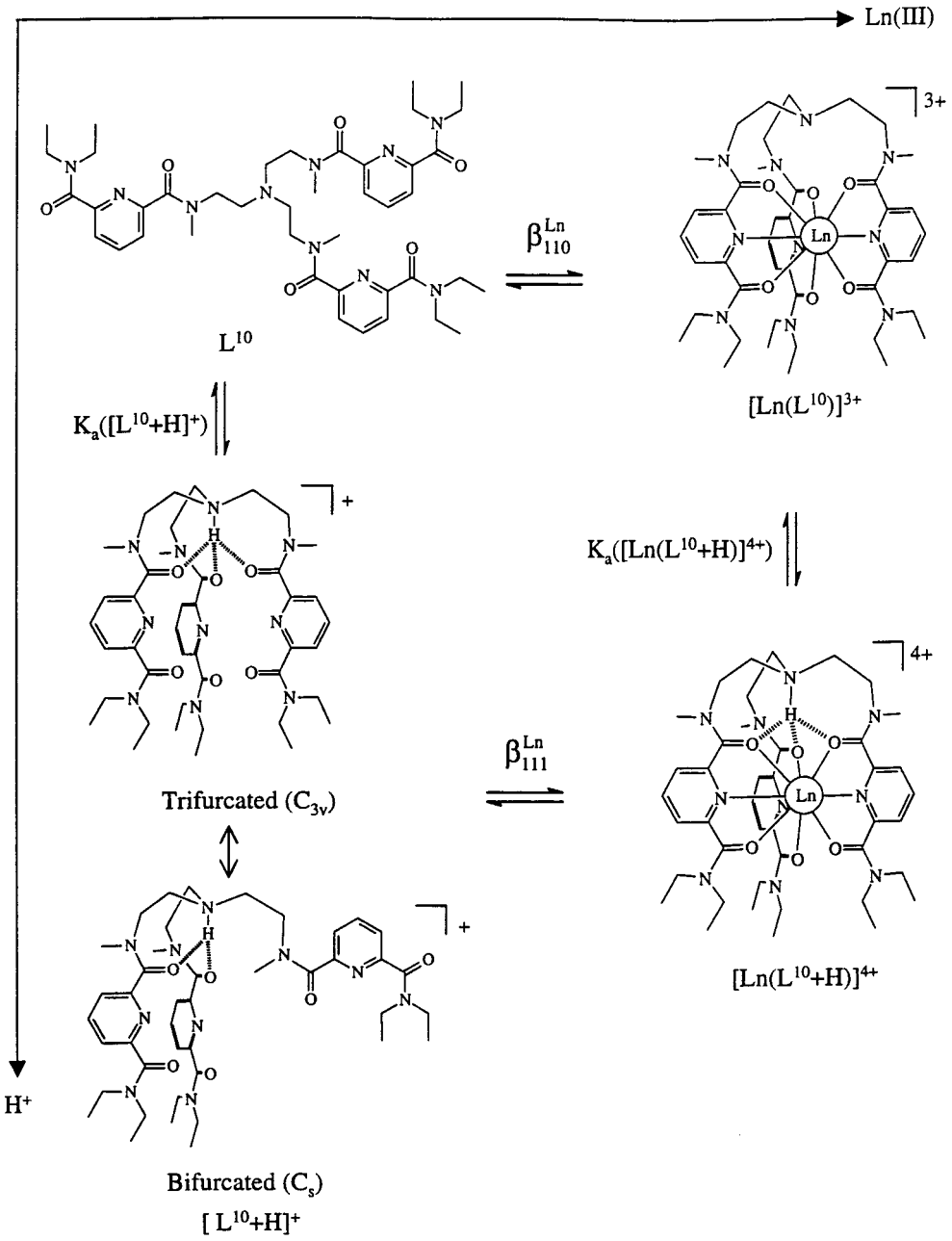

pyridine ring) resulting from their meridional tricoordination to Ln(III). The downfield shift of H^5 in the diamagnetic podates ($\Delta\delta = 0.36-0.41$ ppm, Table 1) confirms the *N*-coordination of the pyridine moiety.[9,27] Contrary to $[La(L^3)_3]^{3+}$ for which a fast P ⇌ M interconversion between helical enantiomers operates in solution leading to sharp NMR signals at 298 K associated with a dynamically averaged D_{3h} symmetry, $[La(L^{10})]^{3+}$ displays only slightly broadened ^{1}H-NMR signals associated with a C_3-symmetrical complex the conformation of which is blocked at room temperature on the NMR time scale. Coalescence to the dynamically averaged C_{3v}-symmetrical structure occurs at 323 K in CD_3CN and points to an improved kinetic inertness for the podate $[La(L^{10})]^{3+}$ compared to the related nonclipped triple-helical complex $[La(L^3)_3]^{3+}$.[9] Addition of an excess of L^{10} to a solution of $[La(L^{10})]^{3+}$ induces a severe broadening of the ^{1}H-NMR signals resulting from intermolecular ligand exchanges at an intermediate rate on the NMR time scale. The podates $[Ln(L^{10})]^{3+}$ (Ln = Y, Lu) which incorporate smaller Ln(III) are significantly less flexible and do not experience fast helical interconversion in the temperature range 273−343 K in acetonitrile. The blocked C_3-symmetrical arrangement of the chelating sidearms is maintained and the addition of an excess of L^{10} has no significant effects on the ^{1}H-NMR spectrum leading to well-separated signals for the free and coordinated ligands. A similar rigidification and improved kinetic inertness with small Ln(III) has been previously noticed for the analogous D_3-symmetrical complexes $[Ln(L^3)_3]^{3+}$.[9]

Further structural information in solution may be gained from the separation of contact (δ_{ij}^{c}) and pseudo-contact (δ_{ij}^{pc}) contributions to the isotropic paramagnetic shift (δ_{ij}^{para}) in axial paramagnetic lanthanide complexes.[12,32] The experimental chemical shift (δ_{ij}^{exp}) for a nucleus *i* in an axial complex of a

(32) (a) Reilley, C. N.; Good, B. W.; Desreux, J. F. *Anal. Chem.* **1975**, *47*, 2110. (b) Reilley, C. N.; Good, B. W.; Allendoerfer, R. D. *Anal. Chem.* **1976**, *48*, 1446. (c) Bertini, I.; Luchinat, C. *NMR of Paramagnetic Molecules in Biological Systems*; Benjamin/Cummings Publishing Co., Menlo Park, CA, 1986; Chapter 10. (d) Bertini, I.; Turano, P.; Vila, A. J. *Chem. Rev.* **1993**, *93*, 2833.

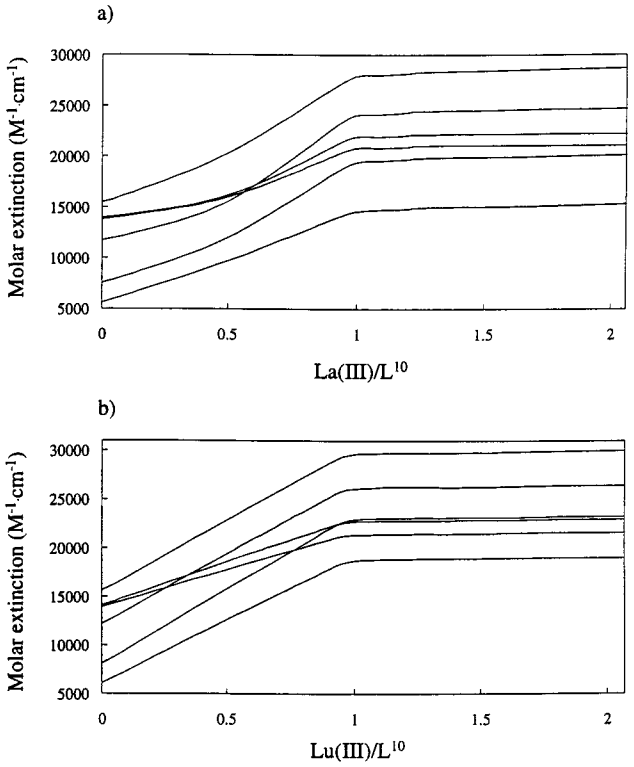

Figure 2. Variation of molar extinction at six different wavelengths for the spectrophotometric titrations of L^{10} (10^{-4} M) with (a) $La(ClO_4)_3 \cdot 6H_2O$ and (b) $Lu(ClO_4)_3 \cdot 7H_2O$ in acetonitrile at 293 K.

Table 2. Cumulative Thermodynamic Formation Constants log (β_{ijk}^{Ln})[a] for the Complexes $[Ln_i(L^{10})_j(H)_k]^{(3+k)+}$ in Acetonitrile and Acetonitrile/Water (95/5, v/v) at 293 K

ion	ionic radius[b]	solvent	log(β_{110}^{Ln})	log(β_{120}^{Ln})	log(β_{111}^{Ln})
La(III)	1.216	CH_3CN	8.3(2)	13.6(2)	6.1(1)
		CH_3CN/H_2O	5.0(1)		4.2(1)
Ce(III)	1.196	CH_3CN	8.5(7)	13.3(9)	
Pr(III)	1.179	CH_3CN	8.0(7)	12.9(9)	
Nd(III)	1.163	CH_3CN	8.1(5)		
Sm(III)	1.132	CH_3CN	7.0(4)		6.7(1)
		CH_3CN/H_2O	6.3(3)		4.9(1)
Gd(III)	1.107	CH_3CN	7.6(4)		
Dy(III)	1.083	CH_3CN	7.4(3)		
Y(III)	1.075	CH_3CN	6.7(4)		6.4(5)
		CH_3CN/H_2O	6.8(1)		5.5(1)
Tm(III)	1.052	CH_3CN	7.2(6)		
Lu(III)	1.032	CH_3CN	8.0(6)		6.4(5)
		CH_3CN/H_2O	7.5(3)		6.1(1)

[a] *i* represents the number of metal ions, *j* the number of ligands, and *k* the number of additional protons in the final podate. [b] Effective ionic radius for nine-coordinate Ln(III).[7]

lanthanide *j* is given by eq 3.[32]

$$\delta_{ij}^{exp} = \delta_{ij}^{para} + \delta_i^{dia} + \delta_j^{bulk} \quad (3)$$

The bulk magnetism δ_j^{bulk} affects similarly all the nuclei in the sample and cancels when using an internal reference (TMS or CD_2HCN).[9,12,33] The isotropic paramagnetic shift (δ_{ij}^{para}) is thus obtained by subtracting the diamagnetic contribution (δ_i^{dia}) taken from the spectra of $[Ln(L^{10})]^{3+}$ (Ln = Y, Lu) from the observed chemical shift of the paramagnetic complexes $[Ln(L^{10})]^{3+}$ (eq 4). In the point approximation, Ln(III) is considered as a paramagnetic dot which allows a straightforward separation of contact (δ_{ij}^{c}, eq 5) and pseudo-contact (δ_{ij}^{pc}, eq 6) contributions in axial complexes (eq 4).[34,35]

$$\delta_{ij}^{para} = \delta_{ij}^{exp} - \delta_i^{dia} = \delta_{ij}^{c} + \delta_{ij}^{pc} \quad (4)$$

$$\delta_{ij}^{c} = \frac{A_i}{\gamma\hbar B_0 T} \cdot \langle S_z \rangle_j = \frac{F_i'}{T} \cdot \langle S_z \rangle_j = F_i \cdot \langle S_z \rangle_j \quad (5)$$

$$\delta_{ij}^{pc} = \frac{k_{CF}}{T^2} \cdot \left(\frac{1 - 3\cos^2\theta_i}{r_i^3} \right) \cdot C_j = \frac{G_i'}{T^2} \cdot C_j = G_i \cdot C_j \quad (6)$$

$\langle S_z \rangle_j$ and C_j are respectively the spin expectation values of S_z and the anisotropic part of the axial magnetic susceptibility tensor which have been tabulated for the free ions.[34−36] The contact term F_i' reflects through-bond Fermi interactions between the paramagnetic center and the nucleus *i* (A_i is the hyperfine interaction parameter and B_0 the applied magnetic induction) which depend on (i) the topological separation of the nucleus *i* and lanthanide *j* and (ii) the mechanism of spin delocalization. The pseudo-contact terms G_i' correspond to through-space effects and depend on the geometric position of the nucleus *i* (r_i and θ_i are the internal axial coordinates with respect to the ligand field axis) and the crystal field parameter (k_{CF}) associated with the complexes. Keeping in mind the Curie (T^{-1}) dependence of F_i and the T^{-2} dependence of G_i and the approximation that $\langle S_z \rangle_j$ and C_j values are the same for free and complexed ions,[34−36] a straightforward calculation of contact and pseudo-contact terms is performed for each nucleus *i* at a fixed temperature according to eq 7 and multilinear least-squares techniques applied to an isostructural series of at least two different axial paramagnetic lanthanide complexes.[9,12,32]

$$\delta_{ij}^{para} = \delta_{ij}^{exp} - \delta_i^{dia} = F_i \cdot \langle S_z \rangle_j + G_i \cdot C_j \quad (7)$$

As previously established for the diamagnetic podates, the paramagnetic complexes $[Ln(L^{10})]^{3+}$ (Ln = Ce, Pr, Nd, Sm, Eu, Yb) display inert C_3-symmetrical structure on the NMR time scale. Obviously, the diastereotopic protons $H^{1,1'}$, $H^{2,2'}$, $H^{7,7'}$, and $H^{9,9'}$ and the quaternary C atoms escape to an unambiguous assignment while C^2, C^7, and C^9 give intricate overlapping signals. Two-dimensional $\{^1H-^1H\}$- and $\{^1H-^{13}C\}$-NMR correlation spectra associated with NOEDIF experiments allow a reliable attribution of the signal arising from H^{3-6}, H^8, and H^{10} and from C^1, C^{3-6}, C^8, and C^{10}, which have been used in the fitting process. The isostructurality of the podates $[Ln(L^{10})]^{3+}$ (Ln = Ce−Yb) along the lanthanide series is checked by plots of $\delta_{ij}^{para}/\langle S_z \rangle_j$ vs $C_j/\langle S_z \rangle_j$ and δ_{ij}^{para}/C_j vs $\langle S_z \rangle_j/C_j$ (two linear forms of eq 7)[36] which are expected to give straight lines for an isostructural series.[37] Analysis of the paramagnetic data for the selected nucleus *i* in $[Ln(L^{10})]^{3+}$ (Table 1) produces approximate straight lines along the complete lanthanide series (Ln = Ce−Yb) pointing to a single structure for these podates in acetonitrile solution (Figure 3). However, the moderate correlation coefficients found for these linear plots point to a rather flexible arrangement of the podand in the complexes which slightly varies with the size of the metal ion. Consequently, the accuracy of the separation of contact (F_i) and pseudo-contact (G_i) terms

(33) (a) Evans, D. F. *J. Chem. Soc.* **1959**, 2003. (b) Evans, D. F.; Fazakerley, G. V.; Phillips, R. F. *J. Chem. Soc. A* **1971**, 1931. (c) Grant, D. H. *J. Chem. Educ.* **1995**, *72*, 39. (d) Piguet, C. *J. Chem. Educ.* **1997**, *74*, 815.

(34) Golding, R. M.; Halton, M. P. *Aust J. Chem.* **1972**, *25*, 2577.

(35) Bleaney, B. *J. Magn. Reson.* **1972**, *8*, 91.

(36) Sherry, D. A.; Geraldes, C. F. G. C. In *Lanthanide Probes in Life, Chemical and Earth Sciences*; Bünzli, J.-C. G., Choppin, G. R., Eds.; Elsevier Publishing Co: Amsterdam, 1989; Chapter 4.

(37) Peters, J. *J. Magn. Reson.* **1986**, *68*, 240.

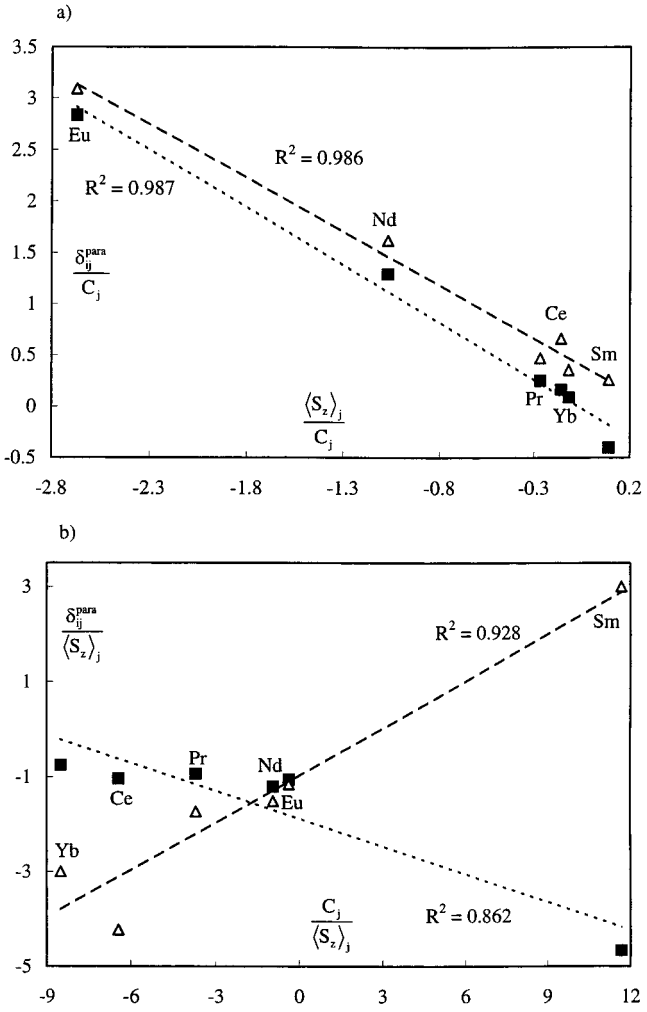

Figure 3. Plots of (a) δ_{ij}^{para}/C_j vs $\langle S_z\rangle_j/C_j$ and (b) $\delta_{ij}^{para}/\langle S_z\rangle_j$ vs $C_j/\langle S_z\rangle_j$ for C^5 in $[Ln(L^{10})]^{3+}$ (■) and $[Ln(L^{10}+H)]^{4+}$ (△) (CD_3CN, 298 K).

is limited as exemplified by the large calculated agreement factors AF_i (eq 8; Table 3).

$$AF_i = \left[\frac{\sum_j (\delta_{ij}^{exp} - \delta_{ij}^{calc})^2}{\sum_j (\delta_{ij}^{exp})^2}\right]^{1/2} \quad (8)$$

Computed values of F_i and G_i terms and AF_i factors are collected in Table 3. Calculated contact and pseudo-contact contributions are given in Table S1 (Supporting Information). If we neglect H^{10} which displays a minor induced paramagnetic shift, the AF_i factors remain large ($0.06 < AF_i < 0.61$) compared to those found for similar mathematical treatments applied to $[Ln(L^3)_3]^{3+}$ ($0.01 < AF_i < 0.31$)[9] and $[Ln(L^1\text{-}2H)_3]^{3-}$ ($0.04 < AF_i < 0.27$).[32a] Large uncertainties affect the F_i and G_i terms (Table 3), but we still observe significant contact terms for the pyridine protons H^{4-6} ($0.10 < F_i < 0.17$) confirming the unusual large spin delocalization onto the aromatic ring previously established for tricoordinated neutral 2,6-disubstituted pyridine units.[9,12] The F_i values for the carbons C^{4-6} are in line with this observation and are similar to those reported for $[Ln(L^3)_3]^{3+}$ [9] pointing to a related meridional tricoordination of the chelating units in the podate $[Ln(L^{10})]^{3+}$. A detailed interpretation of the G_i values is precluded by the limited accuracy of the separation process, but we notice that G_{C^1}, G_{C^3}, and G_{C^4} are positive while G_{C^5} and G_{C^6} are close to zero. This strongly contrasts with the considerable negative values $G_{C^{4,6}} = -0.40(3)$ and $G_{C^5} = -0.22(1)$ found for the D_3-symmetrical complexes $[Ln(L^3)_3]^{3+}$ in which the Ln(III) atom lies in the plane of the three pyridine nitrogen atoms ($\theta_{C^5} = 87°$; $r_{C^5} = 6.31$ Å and $\theta_{C^6} = 108.6°$; $r_{C^{4,6}} = 5.53$ Å taken from the crystal structure of $[Eu(L^3)_3]^{3+}$).[9] A slight shift of Ln(III) out of the plane of the nitrogen atoms of the pyridine rings toward the apical nitrogen atom of the covalent tripod in $[Ln(L^{10})]^{3+}$ increases simultaneously θ_{C^5}, θ_{C^6}, and $r_{C^{5,6}}$ which significantly reduces G_{C^5} and G_{C^6} compared to G_{C^3} and G_{C^4} (eq 6) and accounts for the observed trend in G_i values for the podates $[Ln(L^{10})]^{3+}$.

Formation of the Protonated Podates $[Ln(L^{10}+H)]^{4+}$ (Ln = La−Lu) in Solution. Potentiometric titrations of $[Ln(L^{10})]^{3+}$ with trifluoromethanesulfonic acid (TfOH) in acetonitrile/water (95:5, 0.1 M NBu_4ClO_4) show a single end point corresponding to the formation of a monoprotonated species with $pK_a([Ln(L^{10}+H)]^{4+}) = 3.5(2)$ for Ln = La, Sm, Y, and Lu, within experimental error. ES-MS titrations with TfOH in similar conditions confirm the formation of the protonated complexes $[Ln(L^{10}+H)]^{4+}$ (Table S10, Supporting Information) and the significant downfield shifts of the ^{1}H-NMR signals observed for $H^{1,1'}$ ($\Delta\delta = 1.06-1.22$ ppm) and $H^{2,2'}$ ($\Delta\delta = 0.50-0.68$ ppm) in the diamagnetic protonated podates $[Ln(L^{10}+H)]^{4+}$ (Ln = La, Y, Lu; Table 1) parallel the behavior of $[L^{10}+H]^+$ and imply that protonation involves the apical nitrogen atom of the tripod. Surprisingly, $pK_a([Ln(L^{10}+H)]^{4+})$ is only marginally lower than $pK_a([L^{10}+H]^+)$ (0.8 log unit) despite the larger positive charge borne by the podates. According to the thermodynamic cycle of Scheme 2, $\log(\beta_{111}^{Ln})$ (eq 9) can be estimated using eq 10.

$$Ln^{3+} + [L^{10}+H]^+ \rightleftharpoons [Ln(L^{10}+H)]^{4+} \log(\beta_{111}^{Ln}) \quad (9)$$

$$\log(\beta_{111}^{Ln}) = \log(\beta_{110}^{Ln}) + pK_a([Ln(L^{10}+H)]^{4+}) - pK_a([L^{10}+H]^+) \quad (10)$$

Considering the formation constants $\log(\beta_{110}^{Ln})$ measured in acetonitrile/water (Table 2) and pK_a values obtained in the same conditions, we calculate $\log(\beta_{111}^{Ln}) = 4.2$, 5.5, 6.0, and 6.7 for Ln = La, Sm, Y, and Lu, respectively, which satisfactorily match the experimental values estimated from spectrophotometric titrations of $[L^{10}+H]^+$ with $Ln(ClO_4)_3$ (Table 2). The minor reduction of the formation constants (ca. 0.8 log unit) on going from $[Ln(L^{10})]^{3+}$ to $[Ln(L^{10}+H)]^{4+}$ indicates that the preorganization of the protonated ligand in $[L^{10}+H]^+$ essentially overcomes the increased Coulombic repulsion between the positively charged podand and Ln^{3+}. As previously described for $[Ln(L^{10})]^{3+}$, the formation constants $\log(\beta_{111}^{Ln})$ of $[Ln(L^{10}+H)]^{4+}$ display a small size-discriminating effect along the lanthanide series in acetonitrile/water (95:5) ($\Delta \log(\beta_{111}^{Ln}) = \log(\beta_{111}^{Lu}) - \log(\beta_{111}^{La}) = 1.9$) which disappears in pure acetonitrile (Table 2). Interestingly, no 1:2 complexes can be detected with the protonated podate as a result of the improved electrostatic repulsion between $[Ln(L^{10}+H)]^{4+}$ and a second positively charged podand $[L^{10}+H]^+$.

Structure of the Protonated Podates $[Ln(L^{10}+H)]^{4+}$ (Ln = La−Lu) in Solution. Apart from the shifts of the NMR signals of $H^{1,1'}$, $H^{2,2'}$, C^1, and C^2 associated with the protonation of the apical nitrogen atoms and the appearance in the ^{1}H-NMR spectra of a new broad signal corresponding to the proton of the ammonium group in $[Ln(L^{10}+H)]^{4+}$ (7.85 ppm (Ln = La), 7.60 (Ln = Y), 7.55 (Ln = Lu)), the ^{1}H- and ^{13}C-NMR spectra

Table 3. Computed Values for Contact (F_i) and Pseudo-Contact (G_i) Terms for ^{1}H and ^{13}C Nuclei in Paramagnetic Complexes $[LnL^{10}]^{3+}$ in CD_3CN and $[Ln(L^{10}+H)]^{4+}$ in CD_3CN/CD_3NO_2 (1:1) at 298K

	H^3	H^4	H^5	H^6	H^8	H^{10}	C^1	C^3	C^4	C^5	C^6	C^8	C^{10}
						$[LnL^{10}]^{3+}$							
F_i	0.04(1)	0.13(4)	0.10(4)	0.17(3)	0.01(1)	0.001(2)	0.09(8)	0.08(3)	3.4(4)	−1.1(4)	3.2(3)	−0.1(2)	−0.06(3)
G_i	0.016(6)	−0.02(2)	−0.03(2)	0.01(1)	−0.002(3)	−0.004(7)	0.11(4)	0.01(2)	0.2(2)	−0.04(2)	0.0(1)	0.002(7)	0.01(1)
AF_i	0.44	0.36	0.46	0.27	0.61	0.93	0.54	0.39	0.18	0.06	0.15	0.08	0.44
						$[Ln(L^{10}+H)]^{4+}$							
F_i	−0.01(1)	0.08(7)	0.04(5)	0.1(4)	0.01(1)	0.03(6)	0.2(2)	0.3(6)	2.8(2)	−1.1(1)	3.0(2)	−0.13(1)	−0.01(5)
G_i	−0.00(1)	0.20(4)	0.13(2)	0.10(2)	−0.024(4)	−0.2(3)	−0.41(9)	−0.04(3)	0.4(1)	0.24(4)	0.28(9)	0.00(1)	−0.16(2)
AF_i	0.97	0.31	0.31	0.31	0.24	0.25	0.33	0.30	0.15	0.11	0.12	0.15	0.24

of the diamagnetic podates $[Ln(L^{10}+H)]^{4+}$ (Ln = La, Y, Lu) in CD_3CN/CD_3NO_2 (1:1) display very similar features to those described for the unprotonated analogues (Table 1). The main differences between $[Ln(L^{10}+H)]^{4+}$ and $[Ln(L^{10})]^{3+}$ lie in the dynamic processes occurring in solution which operate at different rates. On the NMR time scale at room temperature, the P ⇌ M helical interconversion is fast for the protonated podate $[La(L^{10}+H)]^{4+}$ leading to an average C_{3v}-symmetry in solution in contrast with the C_3-symmetry found for the more inert podate $[La(L^{10})]^{3+}$. The broad ^{1}H-NMR signals observed for $[Ce(L^{10}+H)]^{4+}$ are compatible with a slower exchange rate and the sharp signals associated with the pairs of diastereotopic protons $H^{1,1'}$ and $H^{2,2'}$ detected for $[Ln(L^{10}+H)]^{4+}$ (Ln = Pr−Lu) are diagnostic for blocked C_3-symmetrical helical structures in solution with small Ln(III) ions. On the other hand, intermolecular exchange between free and complexed ligand is slow for $[Ln(L^{10}+H)]^{4+}$ along the complete lanthanide series as demonstrated by the observation of two sets of sharp aromatic signals in the presence of an excess of ligand. Analysis of the paramagnetic NMR data for $[Ln(L^{10}+H)]^{4+}$ (Ln = Ce−Yb) shows the existence of a single isostructural series since linear plots are obtained for $\delta_{ij}^{para}/\langle S_z\rangle_j$ vs $C_j/\langle S_z\rangle_j$ and δ_{ij}^{para}/C_j vs $\langle S_z\rangle_j/C_j$ (Figure 3). The separation of contact and pseudo-contact contributions is improved ($0.11 < AF_i < 0.31$ except for H^3) compared to that found for $[Ln(L^{10})]^{3+}$ and points to a larger structural rigidity in the protonated podates (Tables 4 and S1). The contact terms (F_i) are alike for $[Ln(L^{10})]^{3+}$ and $[Ln(L^{10}+H)]^{4+}$ in agreement with a similar tridentate binding mode of the chelating units which precludes protonation of the pyridine ring in the latter complexes. A comparison of the G_i terms is difficult because of their complicated dependence on the axial coordinates of the nucleus and the crystal field parameters (eq 6). However, we notice that the absolute G_i values for C^{4-6} are similar ($0.24 < G_i < 0.4$) and in good agreement with those found for the analogous triple-helical complexes $[Ln(L^3)_3]^{3+}$ which indicates a comparable location of the lanthanide ion within the facial plane defined by the C_3-symmetry related nitrogen atoms of the pyridine ring. Compared to $[Ln(L^{10})]^{3+}$ in which Ln(III) is slightly shifted toward the lone pair of the apical nitrogen, protonation in $[Ln(L^{10}+H)]^{4+}$ pushed back Ln(III) toward the center of the pseudo-tricapped trigonal prismatic site defined by the three coordinated tridentate binding units. Since the acidic proton points toward Ln^{III} in $[Ln(L^{10}+H)]^{4+}$ and displays a short Ln···H distance (3.22 Å in the crystal structure of $[Eu(L^{10}+H)]^{4+}$, vide infra), its ^{1}H-NMR signal is very sensitive to paramagnetic effects.[32] Impressive paramagnetic shifts are thus expected e.g. a broad peak at 10.9 ppm corresponding to the proton of the apical ammonium group is observed for the poorly paramagnetic complex $[Sm(L^{10}+H)]^{4+}$ (δ_{Sm}^{para} = 3.3 ppm). The use of paramagnetic lanthanides displaying larger magnetic moments and anisotropies produces a very large paramagnetic shift and a severely increased relaxation rate for the acidic proton which prevents its reliable detection and attribution in $[Ln(L^{10}+H)]^{4+}$ (Ln = Ce−Nd, Eu−Yb).

Isolation of the Podates $[Ln(L^{10})](ClO_4)_3\cdot xH_2O$ [Ln = Eu (4), Gd (5), Tb (6)] and $[Ln(L^{10}+H)](TfO)_4\cdot yH_2O\cdot zCH_3CN$ [Ln = La (7), Eu (8); Gd (9); Tb (10); Lu (11)]. The mixing of stoichiometric quantities of L^{10} and $Ln(ClO_4)_3\cdot xH_2O$ (x = 6−8) in acetonitrile followed by slow diffusion of *tert*-butylmethyl ether produce good yields (83−89%) of amorphous powders whose elemental analyses correspond to $[Ln(L^{10})](ClO_4)_3\cdot xH_2O$ [Ln = Eu, x = 2.5 (**4**), Ln = Gd, x = 2 (**5**); Ln = Tb, x = 2 (**6**)]. IR spectra show the characteristic ligand vibrations (maximum of the band envelope for νC═O at 1650 cm^{-1}) together with two strong bands at 1090 and 625 cm^{-1} typical for ionic perchlorates.[38] Unfortunately, we were unable to obtain X-ray quality crystals for these complexes under various experimental conditions: acetonitrile, propionitrile, butyronitrile, or nitromethane as solvents combined with several diffusing agents (diethyl ether, *tert*-butylmethyl ether, diisopropyl ether) and noncoordinating counteranions (TfO^-, *p*-TsO^-, PF_6^-, BF_4^-, ClO_4^-, $[B(phenyl)_4]^-$). The preparation of the protonated complexes use**s** stoichiometric quantities of L^{10}, trifluoromethanesulfonic acid (TfOH), and $Ln(TfO)_3\cdot xH_2O$ (x = 1.5−5) in acetonitrile/propionitrile (1:1). Diffusion of *tert*-butlymethyl ether into the mixture gives 91−98% of microcrystalline complexes whose elemental analyses correspond to $[Ln(L^{10}+H)](TfO)_4\cdot yH_2O\cdot zCH_3CN$ [Ln = La, y = 0.3, z = 0.2 (**7**); Ln = Eu, y = 0.3, z = 0.2 (**8**); Ln = Gd, y = 0.2, z = 0.3 (**9**); Ln = Tb, y = 0.4, z = 0.1 (**10**); Ln = Lu, y = 0.4, z = 0.1 (**11**)]. IR spectra show the characteristic vibrations of the ligand with a remarkable shift of the maximum of the envelope of the carbonyl stretching toward lower energy (νC═O = 1610 cm^{-1}, $\Delta\nu$ = 40 cm^{-1}) compared to the unprotonated complexes. Weak absorptions corresponding to the cocrystallized solvents (H_2O at 3350−3450 cm^{-1} and CH_3CN at 2260 cm^{-1}) are observed together with the typical vibrations of ionic triflate anions.[39] X-ray quality prisms of $[Eu(L^{10}+H)](CF_3SO_3)_3(PF_6)(CH_3CN)_{0.5}$ (**12**) can be grown from a solution containing a mixture of triflate and hexafluorophosphate counteranions.

Crystal and Molecular Structure of $[Eu(L^{10}+H)](CF_3SO_3)_3(PF_6)(CH_3CN)_{0.5}$ (12). The crystal structure of **12** confirms the existence of a protonated cationic podate $[Eu(L^{10}+H)]^{4+}$ located on a crystallographic 3-fold axis passing through N(1), H(01), and Eu; disordered anions and solvent molecule complete the unit cell (see Experimental Section). Figure 4 shows the numbering scheme of the asymmetric unit and Figure 5 shows ORTEP[40] views of the cation perpendicular to and along the

(38) Nakamoto, K. *Infrared and Raman Spectra of Inorganic and Coordination Coumponds*, 5th ed.; Wiley: New York, 1997; p 199.
(39) Pascal, J.-L.; Hamidi, M. E. M. *Polyhedron* **1994**, *13*, 1787.
(40) Johnson, C. K. *ORTEP II*; Report ORNL-5138; Oak Ridge National Laboratory: Oak Ridge, TN, 1976.

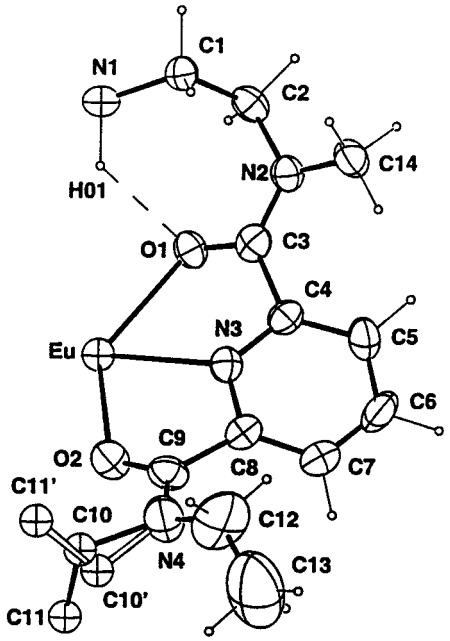

Figure 4. Atomic numbering scheme of the cation $[Eu(L^{10}+H)]^{4+}$ in **12**. Ellipsoids are represented at the 40% probability level. The disordered ethyl group (C10, C11) is represented with arbitrary fixed U_{iso} (0.04 Å^2) for clarity.

3-fold axis. Selected bond distances and bond angles are given in Table 4. Full geometrical parameters, atomic coordinates, and anisotropic displacement parameters are collected in Tables S2−S4 (Supporting Information).

The three chelating units of the podand are tricoordinated to Eu(III) whose coordination sphere is best described as a distorted tricapped trigonal prismatic site in which the six oxygen atoms of the carboxamide units occupy the vertices of the prism and the three pyridine nitrogen atoms cap the rectangular faces. The Eu atom lies almost in the equatorial plane defined by the 3-fold symmetry related nitrogen atoms N(1), N(1′), N(1″) (deviation 0.028(1) Å). Moreover, Eu is located closer to the lower trigonal face of the prism (1.649(1) Å from {O(2), O(2′), O(2″)} and 1.780(1) Å from {O(1), O(1′), O(1″)}). The Eu−N and Eu−O distances are standard,[9] but the triple-helical podate adopts a conical shape that is exemplified by the larger nonbonding O···O distances observed between the oxygen atoms of the lower trigonal face {O(2), O(2′), O(2″)} (O(2)···O(2′) = 3.01 Å, O(1)···O(1′) = 2.80 Å). This contrasts with the cylindrical arrangement of the helical strands found in the related non-clipped complex $[Eu(L^3)_3]^{3+}$ and we conclude that the Me-TREN tripod in $[Eu(L^{10}+H)]^{4+}$ affects the wrapping of the tridentate chelating sidearms about Eu(III). A deeper understanding of these distortions in $[Eu(L^{10}+H)]^{4+}$ requires the detailed analysis of the coordination sphere.[9,13] The flattening of the trigonal prism along the C_3 axis is measured by the θ_i angles between the Eu−O(1^i) vectors or Eu−O(2^i) and the C_3 axis. We obtain $\theta_i = 42.2°$ for the oxygen atoms of the upper face {O(1), O(1′), O(1″)} which is significantly smaller than the values found for (i) the lower trigonal face {O(2), O(2′), O(2″)} ($\theta_i = 46.5°$) in $[Eu(L^{10}+H)]^{4+}$ and (ii) the related unconstricted triple-helical complex $[Eu(L^3)_3]^{3+}$ ($45.8 \le \theta_i \le 48.6°$ calculated according to a pseudo-C_3 axis).[9] This reflects a significant stretching of the trigonal prism toward the covalent tripod and confirms that protonated Me-TREN induces severe steric constraints which bring closer the oxygen atoms of the proximal carboxamide groups {O(1), O(1′), O(1″)}. The deformation of the trigonal prism toward the octahedron is

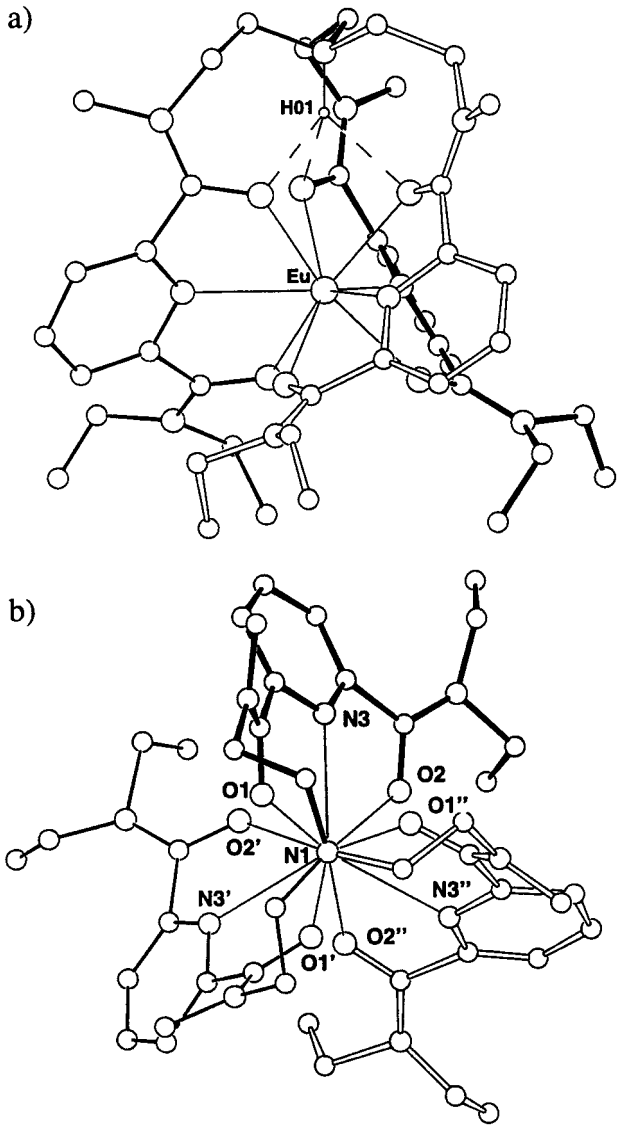

Figure 5. ORTEP[40] views of the cation $[Eu(L^{10}+H)]^{4+}$ (a) perpendicular to the C_3 axis showing the intramolecular trifurcated hydrogen bond and (b) along the C_3 axis showing the helical twist of the complex. Hydrogen atoms have been omitted for clarity.

Table 4. Selected Bond Lengths [Å] and Bond Angles [deg] in $[Eu(L^{10}+H)](CF_3SO_3)_3(PF_6)(CH_3CN)_{0.5}$ (**12**)

Eu−O(1)	2.404(8)	Eu−O(2)	2.395(7)
Eu−N(3)	2.568(7)		
O(1)−Eu−N(3)	63.5(3)	O(1)−Eu−O(2″)	93.2(4)
N(3)−Eu−O(2)	62.4(4)	O(1)−Eu−N(3′)	131.6(3)
O(1)−Eu−O(2)	125.5(2)	O(1)−Eu−N(3″)	78.9(4)
O(1)−Eu−O(1′)	71.2(3)	O(2)−Eu−N(3′)	135.1(2)
O(2)−Eu−O(2′)	77.8(3)	O(2)−Eu−N(3″)	74.5(3)
O(1)−Eu−O(2′)	153.1(4)		

measured by the ω_i angles between the vectors Eu-proj[O(i)] and Eu-proj[N(i)] where proj[O(i)] and proj[N(i)] stand for the projections of the oxygen and nitrogen atoms of the coordination sphere onto a plane perpendicular to the C_3 axis and passing through Eu(III). The interligand ω_i angle between the oxygen atoms of the distal trigonal faces amounts to ω(Eu-proj[O(1)];Eu-proj[O(2′)]) = 21.6° compared with $\omega_i = 14.6-17.1°$ for $[Eu(L^3)_3]^{3+}$ [9] which implies a significant twist of the prism (we expect $\omega_i = 0°$ for a perfect prism and 60° for a perfect octahedron). However, the variable successive intraligand ω_i values are similar (ω(Eu-proj[O(2)];Eu-proj[N(3)]) = 51.0° and

ω(Eu-proj[N(3)];Eu-proj[O(1)]) = 47.4°) and point to a rather regular wrapping of the strands coordinated to Eu(III). Finally, we have resorted to four parallel planes F_{1-4} defined by the symmetry-related atoms of the chelating tridentate binding units to quantify the helical revolution of the threads about the 3-fold axis; F_1 is defined by {O(2), O(2′), O(2″)}, F_2 by {N(3), N(3′), N(3″)}, F_3 by {O(1), O(1′), O(1″)}, and F_4 by {C(1), C(1′), C(1″)}. The separations between these planes d_1 = 1.677(1) Å (F_1-F_2), d_2 = 1.752(1) Å (F_2-F_3), and d_3 = 3.078(1) Å (F_3-F_4) allow the calculation of pitches P_i associated with each helical portion according to $P_i = (d_i/\omega_i)\cdot 360$.[41] $P_1 - P_2$ corresponds to the wrapping of the helical portion containing the coordination sphere while P_3 reflects the helical twist within the covalent tripod. We calculate P_1 = 11.84 Å, P_2 = 13.30 Å, and P_3 = 34.65 Å which correspond to a decrease of the helical torsion when going from the lower oxygen trigonal face (F_1) toward the carbon trigonal face (F_4). It is worth noting that the ligand threads invert their screw direction between the helical portions F_2-F_3 and F_3-F_4 which thus possess opposite helicities leading to an irregular conical amphiverse helix (Figure 5).[42] Similar calculations for the analogous nonclipped cation $[Eu(L^3)_3]^{3+}$ show a regular helical pitch of 11.32 Å between F_1 and F_3. A remarkable trifurcated hydrogen bond is evidenced between atom N(1) (endo conformation) and O(1), O(1′), and O(1″) atoms,[12,43] with a gauche conformation about the C(1)−C(2) bond (dihedral angle: −97.0(9)°, Figure 5). The hydrogen bond length H(01)···O(1) = 2.167(8) Å, (N(1)···O(1) = 3.02-(1) Å) and the bond angle N(1)−H(01)···O(1) = 131.8(4)° are comparable with those found in related podates in which three bidentate catecholate sidearms are organized around six-coordinate Ti(IV)[44] or Ge(IV)[45] by a tris(3-hydroxypropyl)amine tripod. In the latter complexes, the trifurcated hydrogen bond is associated with the formation of three fused nine-membered rings while three fused and helically twisted seven-membered rings (N(1)−C(1)−C(2)−N(2)-C(3)−O(1)−H(01)) in $[Eu(L^{10}+H)]^{4+}$ contribute to the rigidity and the compact arrangement of the tripod.

As the *z* coordinates of the Eu atoms in the unit cell are aproximately *n*/12 (*n* is odd and the difference relative to an exact twelfth amounts to Δ = 0.032 Å), the latter atoms are distributed in almost equidistant planes perpendicular to the *c* axis ($c/6 \pm 2\Delta$ = 10.233 and 10.107 Å). The cations $[Eu(L^{10}+H)]^{4+}$, which are located on 3-fold axes, are distributed in parallel layers in a hexagonal AABBCC close-packed arrangement (Figure 6). Pairs of adjacent layers are related by inversion centers and show *head-to-head* and *tail-to-tail* orientations of the cations with Eu···Eu distances of 12.691(1) and 10.233(2) Å, respectively. TfO^- anions occupy the free space between the conical podates within a *head-to-head* bilayer whereas disordered acetonitrile molecules and hexafluorophosphate anions are located in the interstitial spaces between *head-to-head* and *tail-to-tail* bilayers, respectively.

Photophysical Properties of $[Ln(L^{10}+H)](TfO)_4\cdot yH_2O\cdot zCH_3CN$ [Ln = Eu (8), Gd (9), Tb (10)] and $[Ln(L^{10})](ClO_4)_3\cdot xH_2O$ [Ln = Eu (4), Gd (5), Tb (6)]. In acetonitrile, the ligand L^{10} shows a broad and asymmetric absorption band

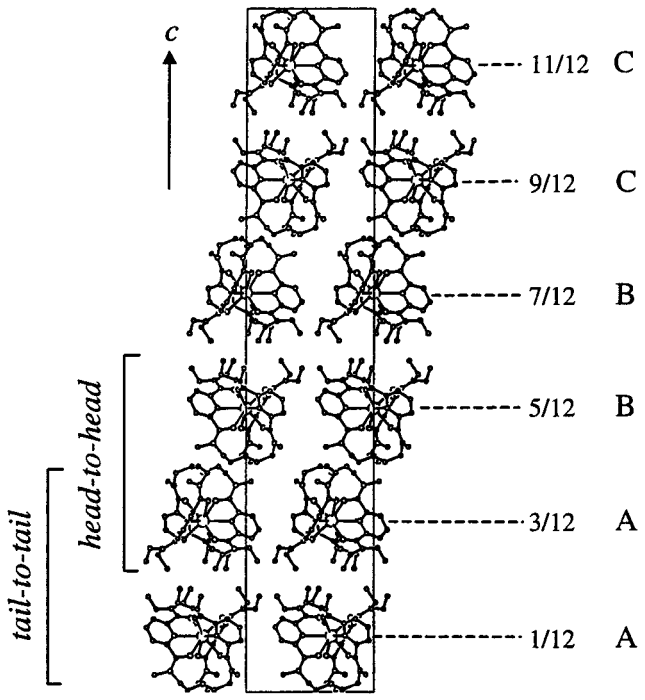

Figure 6. Projection of the unit cell of **12** along the *b* axis showing the hexagonal close-packed AABBCC arrangement of the podates and the location of the *head-to-head* and *tail-to-tail* bilayers (H atoms, anions, and solvent molecules are omitted for clarity).

envelope centered around 37450 cm^{-1} and assigned to a combination of $\pi \rightarrow \pi^*$ and $n \rightarrow \pi^*$ transitions as previously established for L^3 (37040 cm^{-1}).[9] Upon complexation to Ln(III), we observe a structuration of the main absorption band associated with a red shift of the maximum ($\Delta\nu \approx 1350$ cm^{-1}, Ln = Eu, Gd, Tb) and an increase in intensity (Table 5). Very similar absorption spectra are obtained for $[Ln(L^{10})]^{3+}$ and $[Ln(L^{10}+H)]^{4+}$ in complete agreement with the protonation of the apical nitrogen atom which is not involved in the low-energy electronic transitions. Upon irradiation in the UV, we do not detect any significant emission for the free ligand in solution and in the solid state in the temperature range 77−295 K. This points to the existence of efficient nonradiative deactivation pathways as reported for L^3.[9] In the podates $[Gd(L^{10})](ClO_4)_3$ (**5**) and $[Gd(L^{10}+H)](TfO)_4$ (**9**) at 77 K, a weak broad fluorescence band centered at 25000−26000 cm^{-1} is assigned to the emission of the ligand-centered $^1\pi\pi^*$ excited state in view of its removal in time-resolved spectra (delay time ≥50 μs), but we were unable to detect the long-lived emission of the triplet state expected at lower energy for $[Gd(L^{10})](ClO_4)_3$ and $[Gd(L^{10}+H)](TfO)_4$. These poor ligand-centered emission properties parallel those reported for L^3 and its complex $[Gd(L^3)_3](TfO)_3$ ($^1\pi\pi^*$ at 23500 cm^{-1}) and limit the use of such tridentate binding units for the development of efficient luminescent probes.[9] Consequently, the intensities of the emission spectra of $[Eu(L^{10})](ClO_4)_3$ (**4**) and $[Eu(L^{10}+H)](TfO)_4$ (**8**) obtained upon irradiation of the ligand are weak leading to the observation of the metal-centered $^5D_0 \rightarrow {}^7F_j$ (j = 0−4) transitions together with a broad residual emission of the ligand-centered $^1\pi\pi^*$ excited state confirming a poor antenna effect combined with an inefficient $L^{10} \rightarrow$ Eu(III) energy transfer. Nevertheless, the measured intensities at 10 K are strong enough to extract valuable structural information from the high-resolution emission spectra of the Eu(III) complexes (Figure 7).[46]

The emission spectra of $[Eu(L^{10}+H)](TfO)_4$ (**8**) obtained upon irradiation through the ligand-centered excited states (25190

(41) For a related calculation with octahedral d-block helicates see: Charbonnière, L. J.; Williams, A. F.; Piguet, C.; Bernardinelli, G.; Rivara-Minten, E. *Chem. Eur. J.* **1998**, *4*, 485.

(42) Brewster, J. H. *Top. Curr. Chem.* **1974**, *47*, 29.

(43) (a) Taylor, R.; Kennard, O.; Versichel, W. *Acta Crystallogr.* **1984**, *B40*, 280. (b) Taylor, R.; Kennard, O.; Versichel, W. *J. Am. Chem. Soc.* **1983**, *105*, 5761.

(44) Hahn, E. F.; Rupprecht, S.; Moock, K. H. *J. Chem. Soc., Chem. Commun.* **1991**, 224.

(45) Wolff, B.; Weiss, A. *Angew. Chem., Int. Ed. Engl.* **1986**, *25*, 162.

Table 5. Ligand-Centered Absorption[a] in Acetonitrile Solution (295 K) and Ligand-Centered Singlet State Energies As Determined from the Emission Spectra of the Solid at 77 K for L^{10} and Its Complexes $[Ln(L^{10})](ClO_4)_3$ and $[Ln(L^{10}+H)](TfO)_4$

compd	absorption/cm^{-1} $\pi \rightarrow \pi^* + n \rightarrow \pi^*$	emission/cm^{-1} $^1\pi\pi^*$	λ_{exc}/cm^{-1}
L^{10}	37450 (13030)	25000 br	40000
$[Eu(L^{10})]^{3+}$ (**4**)	41670 (29000 sh)	23800 br	37040
	37310 (23500 sh)		
	36100 (25500)		
	35210 (23500 sh)		
$[Gd(L^{10})]^{3+}$ (**5**)	42020 (30000 sh)	25100 br	40000
	37310 (24000 sh)		
	35970 (26000)		
	35090 (24000 sh)		
$[Tb(L^{10})]^{3+}$ (**6**)	41670 (30000 sh)	23810 br	37040
	37310 (24000 sh)		
	36100 (26000)		
	35210 (24000 sh)		
$[Eu(L^{10}+H)]^{4+}$ (**8**)	41840 (30000 sh)	25000 br	40000
	36630 (24000 sh)		
	35970 (27700)		
	35090 (24500 sh)		
$[Gd(L^{10}+H)]^{4+}$ (**9**)	41370 (29700 sh)	26000 br	40000
	37040 (24000 sh)		
	35970 (27500)		
	35090 (24800 sh)		
$[Tb(L^{10}+H)]^{4+}$ (**10**)	42010 (29000 sh)	24390 br	38460
	37450 (24500 sh)		
	36500 (27700)		
	35590 (24800 sh)		

[a] Energies are given for the maximum of the band envelope in cm^{-1} and the molar absorption coefficient (ϵ) is given in parentheses in $M^{-1}\cdot cm^{-1}$; sh = shoulder, br = broad.

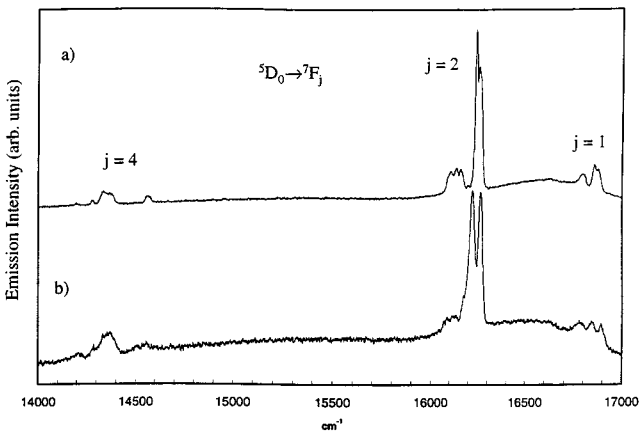

Figure 7. Part of the laser-excited emission spectra of (a) $[Eu(L^{10}+H)](TfO)_4$ (**8**) and (b) $[Eu(L^{10})](ClO_4)_3$ (**4**) at 10 K.

cm^{-1}) or through laser excitation of the $^5D_0 \leftarrow {}^7F_0$ transition are similar and not temperature dependent. The profile of the $^5D_0 \leftarrow {}^7F_0$ transition in the excitation spectrum at 10 K reveals a symmetrical band centered at 17215 cm^{-1} (full width at half-height: fwhh = 11.9 cm^{-1}) compatible with the existence of a single Eu(III) site in the crystal. This transition is shifted to 17225 cm^{-1} at 295 K[46] and matches that previously observed for $[Eu(L^3)_3]^{3+}$ in the same conditions (17227 cm^{-1}).[9] The application of Frey and Horrocks' equation[47] predicts an energy of 17233 cm^{-1} for this transition at 295 K when Eu(III) is nine-coordinate by six oxygen atoms of carboxamide groups and three heterocyclic nitrogen atoms,[9] in qualitative good agreement with the experimental values. A detailed analysis of the high-resolution emission spectrum of $[Eu(L^{10}+H)](TfO)_4$ (**8**) reveals features typical for a C_3-symmetrical environment around Eu(III) (Figure 7a).[9,13,47] Two main components are observed for the $^5D_0 \rightarrow {}^7F_1$ transition which are attributed to the A $\rightarrow$ A (16797 cm^{-1}) and A $\rightarrow$ E components (16856 and 16878 cm^{-1}). The further faint splitting of the A $\rightarrow$ E transition ($\Delta E = 22$ cm^{-1}) results from minor deviation from C_3-symmetry[48] and can be compared to $\Delta E = 20$ cm^{-1} found in $[Eu(L^3)_3](TfO)_3$.[9] The $^5D_0 \rightarrow {}^7F_2$ transition displays three main components (one A $\rightarrow$ A and two A $\rightarrow$ E components) of which the two A $\rightarrow$ E transitions are further split by 18 and 16 cm^{-1}, respectively (16106 cm^{-1}, A $\rightarrow$ A; 16136 and 16158 cm^{-1}, A $\rightarrow$ E; and 16242 and 16258 cm^{-1}, A $\rightarrow$ E). The Eu($^5D_0$) lifetimes of $[Eu(L^{10}+H)](TfO)_4$ (1.78−1.81 ms at 10 K; Table S11 in the Supporting Information) do not depend significantly on the temperature and are only marginally shorter than those measured for $[Eu(L^3)_3](TfO)_3$ (1.83−1.93 ms)[9] pointing to a negligible contribution of the protonated tripod (N−H oscillators) to the deactivation pathways of the Eu($^5D_0$) level.[24,49]

The emission spectrum of the podate $[Eu(L^{10}+H)]^{4+}$ in acetonitrile (10^{-3} M) is very similar to that obtained in the solid state and confirms that the C_3-symmetrical structure is maintained in solution in agreement with NMR data. The Eu($^5D_0$) lifetime is slightly longer in solution (1.96(3) ms) as often observed with related complexes[9,13,12,48] and this confirms that no water molecules are complexed in the first coordination sphere. Although the quantum yield of $[Eu(L^{10}+H)]^{4+}$ relative to $[Eu(terpy)_3]^{3+}$ is weak and amounts to $\Phi_{rel} = 1.1 \times 10^{-2}$ ($\Phi_{abs} = 1.5 \times 10^{-4}$),[50] it corresponds to twice that measured for $[Eu(L^3)_3]^{3+}$ in the same conditions.[9] The protection of Eu^{III} in $[Eu(L^{10}+H)]^{4+}$ and its resistance toward hydrolysis is significantly improved. The addition of 10 M water in acetonitrile has only a minor effect on the emission spectrum of $[Eu(L^{10}+H)]^{4+}$ and its associated Eu($^5D_0$) lifetime (1.96(3) ms in the absence of water and 1.29(5) ms with 10 M water, Table 6), while a drastic quenching of the luminescence is observed for $[Eu(L^3)_3]^{3+}$ after the addition of 1 M water (Figure 8).[9] A comparison between the quenching efficiencies of H_2O vs D_2O using the empirical Horrocks and Sudnick's equation[51] allows a maximum estimation of $q = 0.2 \pm 0.5$ water molecule coordinated to Eu^{III} in acetonitrile containing 10 M water (Table S5). Such a small number can be accounted for by interactions in the second coordination sphere.

The excitation spectrum of the deprotonated podate $[Eu(L^{10})](ClO_4)_3$ (**4**) at 10 K displays two broad bands centered at 17213 and 17236 cm^{-1} pointing to at least two different crystallographic sites in the solid. However, selective laser-excited emission spectra do not show significant variations in agreement with the existence of several sites with very similar geometries resulting from the flexible nature of the unprotonated podand. Despite the faint metal-centered emission of the complex, we detect three equally spaced components for the $^5D_0 \rightarrow {}^7F_1$ transition (16892, 16845, and 16779 cm^{-1}, Figure 7b) implying a severe distortion from C_3-symmetry. The Eu($^5D_0$) lifetime (1.41 ms at 10 K, Table S11) is shorter for $[Eu(L^{10})](ClO_4)_3$ compared to its protonated analogue which strongly suggests a

(46) Bünzli, J.-C. G. In *Lanthanide Probes in Life, Chemical and Earth Sciences*; Bünzli, J.-C. G., Choppin, G. R., Eds.; Elsevier Publishing Co: Amsterdam, 1989, Chapter 7.

(47) Frey, S. T.; Horrocks, W. deW. *Inorg. Chim. Acta* **1995**, *229*, 383.

(48) Piguet, C.; Williams, A. F.; Bernardinelli, G.; Bünzli, J.-C. G. *Inorg. Chem.* **1993**, *32*, 4139.

(49) Aime, S.; Botta, M.; Dickins, R. S.; Maupin, C. L.; Parker, D. A.; Riehl, J. P.; Williams, J. A. G. *J. Chem. Soc., Dalton Trans.* **1998**, 881.

(50) Petoud, S.; Bünzli, J.-C. G.; Glanzman, T.; Piguet, C.; Xiang, Q.; Thummel, R. P. *J. Luminesc.* **1999**, *82*, 69.

(51) (a) Horrocks, W. deW.; Sudnick, D. R. *J. Am. Chem. Soc.* **1979**, *101*, 334. (b) Horrocks, W. deW.; Sudnick, D. R. *Science* **1979**, *206*, 1194. (c) Horrocks, W. deW.; Sudnick, D. R. *Acc. Chem. Res.* **1981**, *14*, 384.

Table 6. Quantum Yields (Φ_{rel}) Relative to $[Eu(terpy)_3]^{3+}$ and $[Tb(terpy)_3]^{3+}$ (terpy = 2,2′:6′,2″-Terpyridine) and Lifetimes (τ) of the $Eu(^5D_0)$ and $Tb(^5D_4)$ Levels for $[Ln(L^{10})](ClO_4)_3$ and $[Ln(L^{10}+H)](TfO)_4$ (Ln = Eu, Tb) 10^{-3} M[a] in Acetonitrile at 298 K

compd	added H_2O (M)	λ_{exc} (nm)	ϵ_{exc} ($M^{-1}\,cm^{-1}$)	τ (ms)	Φ_{rel}[b]	Φ_{abs}
$[Eu(terpy)_3]^{3+}$	0	371	549	2.71(3)	1	1.3×10^{-2} [c]
$[Eu(L^{10}+H)]^{4+}$	0	314	352	1.96(3)	1.1×10^{-2}	1.5×10^{-4}
	2.0	314	382	1.91(3)	8.6×0^{-3}	1.1×10^{-4}
	4.0	314	367	1.50(3)	7.5×0^{-3}	9.9×10^{-5}
	6.0	313	344	1.36(3)	5.5×10^{-3}	7.3×10^{-5}
	8.0	310	350	1.31(3)	3.5×10^{-3}	4.6×10^{-5}
	10.0	306	361	1.29(3)	2.1×10^{-3}	2.8×10^{-5}
$[Eu(L^{10})]^{3+}$	0	316	716	1.66(3)	8.0×10^{-3}	1.1×10^{-4}
	2.0	315	709	1.56(3)	5.3×10^{-3}	7.0×10^{-5}
	4.0	315	702	1.46(3)	4.2×10^{-3}	5.5×10^{-5}
	6.0	314	705	1.42(3)	2.8×10^{-3}	3.7×10^{-5}
	8.0	312	684	1.32(3)	2.2×10^{-3}	2.9×10^{-5}
	10.0	308	719	1.24(3)	1.8×10^{-3}	2.4×10^{-5}
$[Tb(terpy)_3]^{3+}$	0	364	685	1.21(3)	1	4.7×10^{-2} [c]
$[Tb(L^{10}+H)]^{4+}$	0	319	234	1.58(2)	0.73	3.4×10^{-2}
	2.0	319	236	1.52(2)	0.68	3.2×10^{-2}
	4.0	319	248	1.48(2)	0.57	2.7×10^{-2}
	6.0	318	257	1.27(2)	0.42	2.0×10^{-2}
	8.0	315	271	1.16(2)	0.28	1.3×10^{-2}
	10.0	311	281	1.11(2)	0.19	9.1×10^{-3}
$[Tb(L^{10})]^{3+}$	0	322	704	1.11(2)	1.0×10^{-1}	4.8×10^{-3}
	2.0	320	701	1.09(2)	9.9×10^{-2}	4.7×10^{-3}
	4.0	319	702	1.07(2)	9.6×10^{-2}	4.5×10^{-3}
	7.0	318	697	1.06(2)	8.4×10^{-2}	3.9×10^{-3}
	9.0	315	707	1.05(2)	6.9×10^{-2}	3.2×10^{-3}
	10.0	313	703	1.05(2)	6.1×10^{-2}	2.9×10^{-3}

[a] Quantum yields are determined for 10^{-3} M solution to minimize decomplexation. [b] Relative errors on Φ_{rel} are typically 10−15%. [c] Measured relative to an aerated water solution of $[Ru(bipy)_3]^{2+}$ whose absolute quantum yield has been determined.[52]

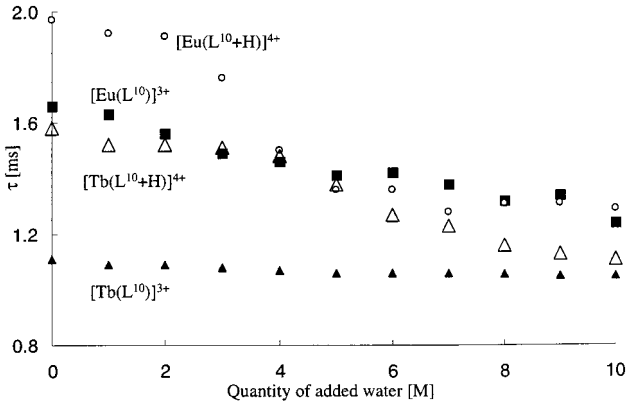

Figure 8. $Eu(^5D_0)$ lifetimes for $[Eu(L^{10}+H)]^{4+}$ (○) and $[Eu(L^{10})]^{3+}$ (■) and $Tb(^5D_4)$ lifetimes for $[Tb(L^{10}+H)]^{4+}$ (△) and $[Tb(L^{10})]^{3+}$ (▲) as a function of the concentration of added water in acetonitrile at 298 K.

less efficient protection of the metallic site from external interactions and/or an improved flexibility of the receptor. According to the excitation spectrum of $[Eu(L^{10})]^{3+}$ in acetonitrile (10^{-3} M, 298 K), a single site is restored in solution whose $^5D_0 \leftarrow {}^7F_0$ transition lies at 17217 cm^{-1} (fwhh = 7.8 cm^{-1}) as similarly found for $[Eu(L^{10}+H)]^{4+}$ (17219 cm^{-1}, fwhh = 9.2 cm^{-1}) and in agreement with a C_3-symmetrical pseudo-tricapped trigonal prismatic coordination geometry around Eu(III). The $Eu(^5D_0)$ lifetime of $[Eu(L^{10})]^{3+}$ (1.66(3) ms) in solution remains shorter than that observed for the analogous protonated podate (1.96(3) ms) thus confirming the better rigidity and protection of the Eu(III) site in $[Eu(L^{10}+H)]^{4+}$. The only marginally lower quantum yields measured for $[Eu(L^{10})]^{3+}$ (Table 6) associated with a similar resistance toward water hydrolysis (Figure 8) unambiguously confirm that (i) the N−H oscillator has minor effects on the emission properties of Eu(III) in $[Eu(L^{10}+H)]^{4+}$ and (ii) the reduced lifetimes observed for $[Eu(L^{10})]^{3+}$ originate from an improved flexibility of the ligand and not from the coordination of water molecules in the first coordination sphere.

As previously reported for the triple-helical complex $[Tb(L^3)_3]^{3+}$,[9] the podates $[Tb(L^{10})]^{3+}$ and especially $[Tb(L^{10}+H)]^{4+}$ exhibit a strong green luminescence upon UV irradiation associated with metal-centered $^5D_4 \rightarrow {}^7F_j$ ($j = 1-6$) transitions. Compared to Eu(III), the quantum yields are more encouraging ($5 \times 10^{-3} < \Phi_{abs} < 5 \times 10^{-2}$) and point to a better $L^{10} \rightarrow$ Tb(III) energy transfer. Resistance toward water hydrolysis is also remarkable with only a minor reduction of the quantum yield upon the addition of 10 M water which can be compared with the 36% decrease observed for $\Phi([Tb(L^3)_3]^{3+})$ in acetonitrile containing 1 M water.

Discussion

The podand L^{10} acts as a nonadentate ligand toward Ln(III) in acetonitrile leading to stable complexes $[Ln(L^{10})]^{3+}$ in which the metal is coordinated in a facial pseudo-tricapped trigonal prismatic site. NMR studies imply that the tridentate chelating units are helically wrapped about Ln(III) to give an isostructural series of C_3-symmetrical podates $[Ln(L^{10})]^{3+}$ (Ln = La−Lu), but the separation of contact and pseudo-contact contributions points to significantly different pseudo-contact terms G_{C^4} and G_{C^6} for the protons located in the meta positions of the pyridine ring. This can be accounted for by a slight shift of Ln(III) toward the covalent tripod associated with a possible weak interaction with the lone pair of the apical nitrogen atom. Emission spectra in solution confirms a C_3-symmetry for $[Eu(L^{10})]^{3+}$ in which Eu(III) is efficiently protected from external interactions. In particular, the $Eu(^5D_0)$ lifetimes measured for $[Eu(L^{10})]^{3+}$ demonstrate that the podate is resistant toward hydrolysis and no water molecule is bound in the first coordination sphere in acetonitrile/water (8:2). As we have firmly established that (i) the podates $[Ln(L^{10})]^{3+}$ possess a similar structure in acetonitrile along the complete lanthanide series and (ii) no extra solvent molecules are coordinated to the metal in $[Ln(L^{10})]^{3+}$, the

complexation process leading to the podate may be reasonably described by two successive *formal* steps: first the complete desolvation of the cation and the ligand (eq 11) followed by the combination of the two desolvated partners (eq 12).[7]

$$[Ln(S)_n]^{3+} + L^{10}(S)_m \rightleftharpoons Ln^{3+} + L^{10} + (m+n)S \quad (11)$$

$$Ln^{3+} + L^{10} \rightleftharpoons [Ln(L^{10})]^{3+} \quad (12)$$

When $S = H_2O$, it has been shown that the opposite enthalpic (ΔH(eq 11) > 0) and entropic ($-T\cdot\Delta S$(eq 11) < 0) contributions to the desolvation process compensate themselves leading to negligible dehydration free energies (ΔG(eq 11) $\approx$ 0) along the complete lanthanide series. Consequently, the variation of free energies for the global complexation process $\Delta G^{global} = \Delta G$(eq 11) + ΔG(eq 12) essentially reflects the combination step (eq 12) leading to the well-known enthalpy-driven electrostatic effect, i.e., an increase of the formation constants with the decreasing size of the lanthanide metal ions.[7] A related behavior is obtained for the formation of $[Ln(L^{10})]^{3+}$ and $[Ln(L^{10}+H)]^{4+}$ in acetonitrile/water (95:5) ($\Delta\log(\beta_{110}^{Ln}) = \log(\beta_{110}^{Lu}) - \log(\beta_{110}^{La}) = 2.5$ and $\Delta\log(\beta_{111}^{Ln}) = \log(\beta_{111}^{Lu}) - \log(\beta_{111}^{La}) = 1.9$, respectively) which suggests that Ln(III) ions are preferentially solvated by water molecules in this solvent. In pure acetonitrile (water content $\leq 10^{-3}$ M), lanthanide perchlorates at low concentrations (10^{-3}–10^{-4} M) exist as solvated ions $[Ln(CH_3CN)_n]^{3+}$ ($n = 8, 9$) whose structures are similar to those found for the aquo ions.[53] We can reasonably assume that the enthalpic contribution to the desolvation process is reduced (ΔH(eq 11)-(CH_3CN) < ΔH(eq 11) (H_2O)) while the entropic terms which essentially reflect the translational contributions[54] are comparable (ΔS(eq 11)(CH_3CN) $\approx$ ΔS(eq 11)(H_2O)) in both solvents. Therefore, the compensation effect observed for the dehydration step in water is removed in pure acetonitrile and we have to consider separately the global enthalpic ($\Delta H^{global} = \Delta H$(eq 11) + ΔH(eq 12)) and entropic contributions ($\Delta S^{global} = \Delta S$(eq 11) + ΔS(eq 12)) to the complexation process for which we cannot foresee straightforward trends. We observe that the free energies for the formation of $[Ln(L^{10})]^{3+}$ (eq 1) and $[Ln(L^{10}+H)]^{4+}$ (eq 9) in acetonitrile do not vary significantly along the lanthanide series suggesting that either ΔH^{global} and ΔS^{global} do not depend on the ionic size of the lanthanides or specific compensations occur between the thermodynamic contributions along the lanthanide series. Surprisingly, the protonation of the apical nitrogen atom of the tripod has only minor effects on the global free energies of complexation, $\log(\beta_{111}^{Ln})$ being only marginally smaller than $\log(\beta_{110}^{Ln})$ for a given lanthanide metal ion despite the increased electrostatic repulsion between the positively charged podand $[L^{10}+H]^+$ and Ln^{3+} (Table 2). According to our detailed NMR and potentiometric studies of L^{10}, we conclude that protonation of the free ligand provides a ca. 1:1 mixture of two clipped conformers which are highly preorganized for the complexation of Ln(III). Bifurcated and trifurcated hydrogen bonds involving the protonated apical nitrogen and the proximal oxygen atoms of the carboxamide groups are thought to stabilize the clipped conformation as exemplified by the observation of such interactions in the crystal structure of $[Eu(L^{10}+H)]^{4+}$.

The clipping of three carboxamide units by a short covalent tripod and the protonation of the apical nitrogen atom in $[Ln(L^{10}+H)]^{4+}$ forces Ln(III) to lie in the center of the pseudo-tricapped trigonal prismatic site and provides a global conical shape for the podate as observed in the crystal structure of $[Eu(L^{10}+H)]^{4+}$. The pseudo-contact terms G_i found for $[Ln(L^{10}+H)]^{4+}$ in solution suggest that a related structure is maintained in solution and we have further tested this hypothesis by using the crystal structure of $[Eu(L^{10}+H)]^{4+}$ as a structural model for the separation of contact and pseudo-contact contributions in $[Ln(L^{10}+H)]^{4+}$ and $[Ln(L^{10})]^{3+}$ in solution. We have complied to the following procedure. (1) Starting from the axial coordinates θ_i and r_i for each nucleus H^{4-6}, C^1, C^{3-6}, C^8, C^{10} taken from the crystal structure of $[Eu(L^{10}+H)]^{4+}$, the structural factors $(1 - 3\cos^2\theta_i)/r_i^3$ are calculated (the protons H^3, H^8, and H^{10} are not considered because of fast rotation of the methyl groups in solution). (2) Contact contributions are excluded for C^1, C^8, and C^{10} which are sufficiently remote from the Ln(III) site and which possess small to negligible F_i terms (Table 3). (3) The experimental isotropic paramagnetic shifts (δ_{ij}^{para}) are fitted to eq 13 by using multilinear least-squares methods with eight parameters for each lanthanide j (seven contact contributions (δ_{ij}^{c} for H^{4-6} and C^{3-6}) and one axial anisotropic magnetic susceptibility parameter ($\xi\cdot\chi_j^{zz}$), 10 × 8 fits).[55]

$$\delta_{ij}^{para} = \xi\cdot\chi_j^{zz}\cdot\left(\frac{1 - 3\cos^2\theta_i}{r_i^3}\right) + \sum_i \delta_{ij}^{c} \quad (13)$$

Computed values of $\xi\cdot\chi_j^{zz}$ and δ_{ij}^{c} together with associated average values calculated for F_i and G_i terms using eqs 5 and 6 for $[Ln(L^{10}+H)]^{4+}$ and $[Ln(L^{10})]^{3+}$ (Ln = Ce, Pr, Nd, Sm, Eu, Yb) are given in Tables S6–S8 (Supporting Information). As expected from the increase of adjustable parameters per lanthanide used in this method, the agreement factors AF_i are significantly improved except for C^1, C^8, and C^{10} whose contact contributions are fixed to zero (Table S7, Supporting Information). A comparison of the average F_i and G_i terms obtained by this technique (Tables S8, Supporting Information) with those obtained using eq 7 (Table 3) shows that a satisfying correlation is only observed for $[Ln(L^{10}+H)]^{4+}$ as demonstrated by the Willcott agreement factors (eq 14)[32a] calculated for G_i terms which amounts to 0.46 for $[Ln(L^{10}+H)]^{4+}$ and 1.11 for $[Ln(L^{10})]^{3+}$. As expected, the F_i terms are less sensitive to minor structural changes and good correlation is found for both types of podates in solution ($AF_{F_i} = 0.09$).

$$AF_{G_i} = \left[\frac{\sum_i (G_i^{eq13} - G_i^{eq7})^2}{\sum_i (G_i^{eq7})^2}\right]^{1/2}$$

$$AF_{F_i} = \left[\frac{\sum_i (F_i^{eq13} - F_i^{eq7})^2}{\sum_i (F_i^{eq7})^2}\right]^{1/2} \quad (14)$$

Although a perfect correlation is precluded by the poor rigidity of the podates along the lanthanide series, the expected theoretical trend in axial anisotropic magnetic susceptibility

(52) Nakamaru, K. *Bull. Chem. Soc. Jpn.* **1982**, *55*, 2697.

(53) Deacon, G. B.; Görtler, B.; Junk, P. C.; Lork, E.; Mews, R.; Petersen, J.; Zemva, B. *J. Chem. Soc., Dalton Trans.* **1998**, 3887. Bünzli, J.-C. G.; Milicic-Tang, A. In *Handbook on the Physics and Chemistry of Rare Earthes*; Gschneidner, K. A., Jr., Eyring, L., Eds; Elsevier Science Pub.: Amsterdam, 1995; Vol. 21, Chapter 145.

(54) Mammen, M.; Shakhnovich, E. I.; Deutch, J. M.; Whitesides, G. M. *J. Org. Chem.* **1998**, *63*, 3821.

(55) Kemple, M. D.; Ray, B. D.; Lipkowitz, K. B.; Prendergast, F. G.; Rao, B. D. N. *J. Am. Chem. Soc.* **1988**, *110*, 8275.

Table 7. Comparison between Theoretical and Experimental Data of the Principal Value of the Axial Anisotropic Magnetic Susceptibility Tensor ($\xi \cdot \chi_j^{zz}$) for $[Ln(L^{10})]^{3+}$ and $[Ln(L^{10}+H)]^{4+}$ in Solution[a]

Ln_j	theory[35]	$[Ln(L^{10})]^{3+}$	$[Ln(L^{10}+H)]^{4+}$
Ce	0.57	−0.08	1.33
Pr	1.00	1.00	1.00
Nd	0.38	−0.36	1.22
Sm	0.06	0.15	0.12
Eu	−0.36	0.05	−0.69
Yb	−2.00	−0.80	−2.25

[a] Ratios relative to Pr(III) are given.[55]

parameter $\xi \cdot \chi_j^{zz}$ is better reproduced for $[Ln(L^{10}+H)]^{4+}$ than for $[Ln(L^{10})]^{3+}$ (Table 7) and we conclude that the crystal structure of $[Eu(L^{10}+H)]^{4+}$ is a satisfying structural model only for $[Ln(L^{10}+H)]^{4+}$ (Ln = La−Lu) in solution. The slight shift toward the apical nitrogen atom of the tripod experienced by Ln(III) in $[Ln(L^{10})]^{3+}$ produces a new set of structural factors $(1 - 3\cos^2\theta_i)/r_i^3$ which significantly deviate from those observed in the crystal structure of $[Eu(L^{10}+H)]^{4+}$.

However, the improved kinetic inertness toward P ⇌ M helical interconversion observed for $[Ln(L^{10})]^{3+}$ compared to $[Ln(L^{10}+H)]^{4+}$ in solution is difficult to attribute to such minor structural variations. Raymond and co-workers have studied similar interconversion processes for triple-helical complexes containing six-coordinate Ga(III) and conclude that Bailar twists involving trigonal prismatic transition states with no bond breaking are operating.[56] For nine-coordinate podates $[Ln(L^{10}+H)]^{4+}$ and $[Ln(L^{10})]^{3+}$, a related torsion mechanism would involve an eclipsed trigonal prism as the transition state which will produce severe steric constraints within the tripod and considerable repulsion between the terminal carboxamide groups of the chelating units. An alternative mechanism involving a partial decomplexation of one or more chelate sidearms appears more likely as demonstrated by Williams and co-workers for sterically constrained bimetallic triple-stranded helicates.[57] According to this mechanism, the larger stability found for $[Ln(L^{10})]^{3+}$ compared to $[Ln(L^{10}+H)]^{4+}$ may account for its improved kinetic inertness since a tighter binding of the chelating units is expected in $[Ln(L^{10})]^{3+}$.

In view of the poor light-harvesting properties of the pyridine-2,6-dicarboxamide binding units,[9] these podates present only limited interest as light-converting devices. However, laser-excited high-resolution emission spectra confirm the C_3-symmetrical structure adopted by $[Eu(L^{10}+H)]^{4+}$, while significant distortions are observed for $[Eu(L^{10})]^{3+}$ in the solid state. According to $Eu(^5D_0)$ lifetimes, strong interactions with water molecules are excluded for both complexes in acetonitrile containing up to 10 M water which represents a significant improved resistance toward water hydrolysis compared to the related nonclipped triple-helical complex $[Eu(L^3)_3]^{3+}$.[9]

Conclusion

The simultaneous control of (i) the mutual orientation of three unsymmetrical meridionally tricoordinated semirigid bent tridentate chelating units and (ii) their wrapping around spherical nine-coordinate Ln(III) ions has been achieved through the connection of pyridine-2,6-dicarboxamide sidearms to the tris-(2-(*N*-methyl)aminoethyl)amine tripod resulting in stable C_3-symmetrical podates $[Ln(L^{10})]^{3+}$ and $[Ln(L^{10}+H)]^{4+}$. The crystal structure of $[Eu(L^{10}+H)]^{4+}$ reveals that the protonated apical nitrogen atom of the tripod adopts an endo conformation leading to a trifurcated hydrogen bond involving the three surrounding oxygen atoms of the proximal carboxamide units as acceptors and causing a stretching of the trigonal prism toward the covalent tripod. Although we were not able to obtain a crystal structure for $[Ln(L^{10})]^{3+}$, the solution structure established by paramagnetic NMR indicates that $[Ln(L^{10})]^{3+}$ podates display a structure similar to that found for $[Eu(L^{10}+H)]^{4+}$ in the solid state while a slight shift of Ln(III) along the C_3 axis toward the apical nitrogen atom of the covalent tripod is observed for $[Ln(L^{10})]^{3+}$. Therefore, protonation of L^{10} is thought to play a crucial role for (i) preorganizing the free ligand prior to its complexation and (ii) forcing Ln(III) to occupy a central position within the conical facial pseudo-tricapped trigonal prismatic site. This behavior parallels that reported for $[Ln(L^9)]^{3+}$ whose lanthanide metal ion is shifted toward the terminal acetal groups when Ni(II) is introduced within the tripod to give $[LaNi(L^9\text{-}3H)(H_2O)]^{2+}$.[17] In the latter complex, the tripod is rigidified by three fused eight-membered metal-containing macrocycles, while three fused seven-membered hydrogen-containing macrocycles are produced in $[Ln(L^{10}+H)]^{4+}$. It is worth noting that each tridentate sidearm in $[Ln(L^{10})]^{3+}$ and $[Ln(L^{10}+H)]^{4+}$ provides two-fused five-membered chelate metallacycles incorporating Ln(III) and leading to a slightly distorted tricapped trigonal prismatic site similar to those found in $[Ln(L^i)_3]^{3+}$ (i = 3, 4).[9,13,48] The predicted preference of large Ln(III) ions for five-membered metallacycles[19] is confirmed by our results and may explain the failure to prepare regular triple helical nine-coordinate lanthanide podates with L^{7-9} which are designed to provide fused six-membered chelate metallacycles.[15−19]

When we compare L^{10} with its nonclipped acyclic precursor L^3, the introduction of a covalent tripod brings three major improvements. (1) The strictly facial organization of unsymmetrical tridentate binding units provides a vectorial arrangement of the strands which offers fascinating possibilities for the design of anchors in functional heteropolymetallic lanthanide-containing supramolecular complexes. Directional energy and/or electron transfers require such structural control which is intensively explored for d-block metal ions,[14b,58] but essentially ignored with f-block ions.[1,59] (2) Structural control, thermodynamic stability, and kinetic inertness are improved in $[Ln(L^{10})]^{3+}$ and $[Ln(L^{10}+H)]^{4+}$. Moreover, a fine-tuning of the arrangement of the chelating strands and, consequently, of the size and geometry of the coordination site may be triggered by the protonation of the covalent tripod. The use of alkali or alkaline earth cations as alternative messengers for controlling the lanthanide coordination site is an attracting possibility which is currently being investigated in our laboratories. (3) The clipping of one end of the trigonal prism by a covalent tripod in the podates $[Ln(L^{10})]^{3+}$ and $[Ln(L^{10}+H)]^{4+}$ has a beneficial effect on the protection of the central metal ions toward external interactions, and in particular water is excluded from the first coordination sphere. This is crucial for the design of luminescent devices based on lanthanide metal ions which are very sensitive to deactivation via high-energy NH or OH oscillators.

(56) Meyer, M.; Kersting, B.; Powers, R. E.; Raymond, K. N. *Inorg. Chem.* **1997**, *36*, 5179. Kersting, B.; Meyer, M.; Powers, R. E.; Raymond, K. N. *J. Am. Chem. Soc.* **1996**, *118*, 7221. Kersting, B.; Telford, J. R.; Meyer, M.; Raymond. K. N. *J. Am. Chem. Soc.* **1996**, *118*, 5712.

(57) Charbonnière, L. J.; Gilet, M.-F.; Bernauer, K.; Williams, A. F. *Chem. Commun.* **1996**, 39. Charbonnière, L. J.; Williams, A. F.; Frey, U.; Merbach, A. E.; Kamalaprija, P.; Schaad, O. *J. Am. Chem. Soc.* **1997**, *119*, 2488.

(58) For reviews see: Ward, M. D. *Chem. Soc. Rev.* **1997**, *26*, 365. Von Zelewsky, A.; Belser, P. *Chimia* **1998**, *52*, 620.

(59) Piguet, C.; Bünzli, J.-C. G.; Bernardinelli, G.; Hopfgartner, G.; Williams, A. F. *J. Am. Chem. Soc.* **1993**, *115*, 8197. Bünzli, J.-C. G.; Froidevaux, P.; Piguet, C. *New J. Chem.* **1995**, *19*, 661 and references therein.

Experimental Section

Solvents and starting materials were purchased from Fluka AG (Buchs, Switzerland) and used without further purification, unless otherwise stated. Acetonitrile, dichloromethane, *N*,*N*-dimethylformamide (DMF), and triethylamine were distilled from CaH_2 and thionyl chloride from elemental sulfur. Tris(2-(*N*-methylamino)ethyl)amine (**2**)[25] and 6-(*N*,*N*-diethylcarbamoyl)pyridine-2-carboxylic acid (**3**)[12a] were prepared according to literature procedures. The perchlorate salts $Ln(ClO_4)_3 \cdot nH_2O$ and trifluoromethanesulfonate salts $Ln(OTf)_3 \cdot nH_2O$ (Ln = La to Lu) were prepared from the corresponding oxides (Glucydur, 99.99%) according to literature procedures.[60] Silicagel (Merck 60, 0.040−0.060 mm) was used for preparative column chromatography.

Preparation of Tris{2-[*N*-methylcarbamoyl-(6-(*N*,*N*-diethylcarbamoyl)pyridine-2)ethyl]amine} (L^{10}). A solution of 6-(*N*,*N*-diethylcarbamoyl)pyridine-2-carboxylic acid (**3**, 2.00 g, 9.0 mmol), thionyl chloride (9.8 mL, 0.14 mol), and *N*,*N*-dimethylformamide (100 μL) in dry dichloromethane (80 mL) was refluxed for 45 min. The resulting mixture was evaporated to dryness, coevaporated twice with dichloromethane (2 × 20 mL), and dried under vacuum. The white residual powder was dissolved in dichloromethane, then tris(2-(*N*-methylamino)-ethyl)amine (**2**, 424 mg, 2.25 mmol) and triethylamine (6.3 mL, 45.2 mmol) in dichloromethane (20 mL) were added dropwise under an inert atmosphere. The mixture was refluxed for 90 min, evaporated to dryness, and partitioned between dichloromethane (100 mL) and half-saturated aqueous NH_4Cl (100 mL). The aqueous phase was extracted with dichloromethane (3 × 50 mL) and the combined organic fractions were dried (Na_2SO_4) evaporated to dryness and the crude product was purified by column chromatography (Silicagel; CH_2Cl_2/MeOH 98:2 → 90:10) to give 1.62 g (1.94 mmol, yield 86%) of $L^{10} \cdot 2H_2O$ as a pale yellow oil. ^{1}H NMR in DMSO-d_6 (300 MHz, T = 440 K): δ 1.13 (t, ^3J = 7.0 Hz, 18H), 2.65−2.75 (m, 6H), 2.96 (s, 9H), 3.40 (q, ^3J = 7 Hz, 12H), 3.40 (m, 6H), 7.50−7.58 (m, 6H), 7.95 (t, ^3J = 7 Hz, 3H). ^{13}C NMR in DMSO-d_6 (75 MHz, T = 440 K): primary C 12.39, 34.50; secondary C 40.32, 46.45, 51.11; tertiary C 121.84, 122.17, 137.08; quaternary C 152.93, 153.32, 166.46, 166.89. ES-MS (CH_2Cl_2 + 0.1% HCOOH): m/z 801.4 $[M + H]^+$, 401.6 $[M + 2H]^{2+}$. Thermogravimetry 55−140 °C, weight loss 4.12%, calcd for $2H_2O$ in $C_{42}H_{60}N_{10}O_6 \cdot 2H_2O$: 4.30%.

Preparation of the Complexes $[Ln(L^{10})](ClO_4)_3 \cdot xH_2O$ [Ln = Eu (4), Gd (5), Tb (6)]. $L^{10} \cdot 2H_2O$ (48 mg, 0.06 mmol) and $Ln(ClO_4)_3 \cdot xH_2O$ (Ln = Eu, Gd, Tb; x = 4−7, 0.06 mmol) were dissolved in hot acetonitrile (5 mL). The mixture was cooled and stirred for 1 h at room temperature. Slow diffusion of *tert*-butlymethyl ether for 24 h into the concentrated acetonitrile solution gave 83−86% of complexes $Ln(L^{10})](ClO_4)_3 \cdot xH_2O$ [Ln = Eu, x = 2.5 (**4**), Ln = Gd, x = 2 (**5**), Ln = Tb, x = 2 (**6**)] as white waxy solids.

Preparation of the Complexes $[Ln(L^{10}+H)](TfO)_4 \cdot yH_2O \cdot zCH_3CN$ [Ln = La (7), Eu (8), Gd (9), Tb (10), Lu (11)]. $L^{10} \cdot 2H_2O$ (48 mg, 0.06 mmol) and $Ln(TfO)_3 \cdot xH_2O$ (Ln = La, Eu, Gd, Tb, Lu; x = 1−4, 0.06 mmol) were dissolved in hot acetonitrile/propionitrile (1:1, 5 mL). A 0.06 M solution of trifluoromethanesulfonic acid in acetonitrile (1 mL, 0.06 mmol) was added and *tert*-butlymethyl ether was slowly diffused into the mixture for 3 days to give 91−98% of complexes $[Ln(L^{10}+H)](TfO)_4 \cdot yH_2O \cdot zCH_3CN$ [Ln = La, y = 0.3, z = 0.2 (**7**), Ln = Eu, y = 0.3, z = 0.2 (**8**), Ln = Gd, y = 0.2, z = 0.3 (**9**), Ln = Tb, y = 0.4, z = 0.1 (**10**), Ln = Lu, y = 0.4, z = 0.1 (**11**)] as white microcrystals. X-ray quality crystals of $[Eu(L^{10}+H)](CF_3SO_3)_3(PF_6)(CH_3CN)_{0.5}$ (**12**) were obtained with the same procedure, but tetrabutylammoniumhexafluorophosphate (271 mg, 0.7 mmol) was added to the acetonitrile solution prior to the slow diffusion of diethyl ether. Complexes **4**−**11** were characterized by their IR spectra and gave satisfactory elemental analyses (Table S9, Supporting Information).

Physicochemical Measurements. Electronic spectra in the UV−visible range were recorded at 20 °C from 10^{-3}−10^{-4} M acetonitrile solutions with Perkin-Elmer Lambda 5 and 9 spectrometers using quartz cells of 0.1 and 1 cm path length. Spectrophotometric titrations were performed with a Perkin-Elmer Lambda 5 spectrometer connected to an external computer. In a typical experiment, 50 mL of ligand L^{10} (10^{-4} M) in acetonitrile were titrated at 298 K with a solution of $Ln(ClO_4)_3 \cdot xH_2O$ 2 mM in acetonitrile. After each addition of 0.1 mL, the absorption spectra were recorded using a 1 cm quartz cell and transferred to the computer. Plots of absorbance as a function of the metal/ligand ratio gave a first indication of the number and stoichiometry of the complexes formed; factor analysis was then applied to the data to confirm the number of different absorbing species, and finally, a model for the distribution of species was fitted with a nonlinear least-squares algorithm to give stability constants using the SPECFIT program.[31] IR spectra were obtained from KBr pellets with a Perkin-Elmer 883 spectrometer. Potentiometric titrations were performed under an inert atmosphere in a thermostated titration vessel (298 K) equipped with a pH electrode Metrohm 6.0202.000 connected to a pH meter Metrohm 691. In a typical experiment, 50 mL of ligand L^{10} or complexes $[Ln(L^{10})]^{3+}$ (10^{-3} M) in acetonitrile/water (95:5) containing NBu_4ClO_4 (0.1 M) were titrated with a solution of trifluoromethanesulfonic acid 0.05 M in the same solvent. After each addition of 0.05 mL, the pH was recorded and transferred to a computer. A model for the distribution of species was fitted with a nonlinear least-squares algorithm to give acid−base constants. ^{1}H and ^{13}C NMR spectra were recorded at 298 K on a Broadband Varian Gemini 300 spectrometer. Chemical shifts are given in ppm wrt TMS. EI-MS (70 eV) were recorded with VG-7000E and Finnigan-4000 instruments. Pneumatically assisted electrospray (ES-MS) mass spectra were recorded from 2 × 10^{-4} M acetonitrile solution for the complexes on an *API III* tandem mass spectrometer (PE Sciex). The spectra were recorded under low up-front declustering or collision induced dissociation (CID) conditions, typically ΔV = 0−30 V between the orifice and the first quadrupole of the spectrometer.[61] The experimental procedures for high-resolution, laser-excited luminescence measurements have been published previously.[13,62] Solid state samples were finely powdered and low temperature (77 or 10 K) was achieved by means of a Cryodyne Model 22 closed-cycle refrigerator from CTI Cryogenics. Luminescence spectra were corrected for the instrumental function, but not excitation spectra. Lifetimes are averages of at least 3−5 independent determinations. Ligand excitation and emission spectra were recorded on a Perkin-Elmer LS-50B spectrometer equipped for low-temperature measurements. The relative quantum yields were calculated using the following formula:[13] $Q_x/Q_r = \langle A_r(\lambda_r)/A_x(\lambda_x)\rangle\langle I(\lambda_r)/I(\lambda_x)\rangle\langle n^2_x/n^2_r\rangle\langle D_x/D_r\rangle$ where subscript r stands for the reference and x for the samples; A is the absorbance at the excitation wavelength, I is the intensity of the excitation light at the same wavelength, n is the refractive index (1.341 for all solutions in acetonitrile), and D is the measured integrated luminescence intensity. Thermogravimetric analyses were performed with a Seiko TG/DTA 320 thermogravimetric balance (under N_2). Elemental analyses were performed by Dr. H. Eder from the Microchemical Laboratory of the University of Geneva.

X-ray Crystal Structure Determination of $[Eu(L^{10}+H)](CF_3SO_3)_3(PF_6)(CH_3CN)_{0.5}$ (12). M_r = 1566.6; μ = 9.43 mm^{-1}, $F(000)$ = 4758, D_c = 1.67 g·cm^{-3}, trigonal, $R\bar{3}$, Z = 6, a = 13.2949(5) Å, c = 61.020(3) Å, V = 9340.6(8) Å^3, from 25 reflections (45° < 2θ < 60°), colorless prism 0.12 × 0.23 × 0.44 mm mounted on a quartz fiber with RS3000 oil. Cell dimensions and intensities were measured at 200 K on a Stoe STADI4 diffractometer with graphite-monochromated CuKα radiation (λ = 1.5418 Å), ω−2θ scans, scan width 1.05° + 0.35 tan θ, and scan speed 0.06 deg/s. Two reference reflections measured every 45 min showed no variation. −12 < h <12; 0 < k < 13; 0 < l < 64 and all antireflections; 5097 measured reflections, 2552 unique reflections of which 2179 were observables ($|F_o| > 4\sigma(F_o)$); R_{int} for equivalent reflections 0.049. Data were corrected for Lorentz and polarization effects and for absorption[63] (A^* min, max = 2.725, 7.791). The structure was solved by direct methods using MULTAN 87,[64] all other calculations used the XTAL[65] system. Full-matrix least-

(60) Desreux, J. F. In *Lanthanide Probes in Life, Chemical and Earth Sciences*; Bünzli, J.-C. G., Choppin, G. R., Eds.; Elsevier Publishing Co: Amsterdam, 1989; Chapter 2.

(61) Hopfgartner, G.; Piguet, C.; Henion, J. D. *J. Am. Soc. Mass Spectrom.* **1994**, *5*, 748.

(62) Piguet, C.; Williams, A. F.; Bernardinelli, G.; Moret, E.; Bünzli, J.-C. G. *Helv. Chim. Acta* **1992**, *75*, 1697. Petoud, S.; Bünzli, J.-C. G.; Schenk, K. J.; Piguet, C. *Inorg. Chem.* **1997**, *36*, 1345.

(63) Blanc, E.; Schwarzenbach, D.; Flack, H. D. *J. Appl. Crystallogr.* **1991**, *24*, 1035.

squares refinement based on F using the weight of $1/[\sigma^2(F_o) + 0.0001(F_o^2)]$ gave final values $R = 0.065$, $\omega R = 0.062$, and $S = 2.33(4)$ for 285 variables and 2179 contributing reflections. The non-H atoms were refined with anisotropic displacement parameters except for the two C atoms of one disordered ethyl residue. H-atoms were placed in calculated positions and contributed to F_c calculations. The final difference electron density map showed a maximum of +0.98 and a minimum of −1.02 eÅ^{-3}. The complex is located on a 3-fold axis with Eu, N(1), and H(01) in special positions 6c. One of the ethyl substituents (C(10)−C(11)) shows a cross disorder (population parameters of 0.6 and 0.4) and four atomic sites have been refined with U_{iso} and restraints on bond lengths and bond angles. The PF_6 and CH_3CN molecules are disordered. Crystallographic data (excluding structure factors) have been deposited to the Cambridge Crystallographic Data Base (deposition No. 102293).

Acknowledgment. We gratefully acknowledge V. Foiret for her technical assistance. C.P. thanks the Werner Foundation for a fellowship and J.-C.B. thanks the Fondation Herbette (Lausanne) for the gift of spectroscopic equipment. This work is supported through grants from the Swiss National Science Foundation.

Supporting Information Available: Table S1 lists the computed contact and pseudocontact contribution to the NMR paramagnetic shifts of $[Ln(L^{10})]^{3+}$ and $[Ln(L^{10}+H)]^{4+}$ according to eq 7; atomic coordinates, bond distances and bond angles, and anisotropic displacements parameters for $[Eu(L^{10}+H)](CF_3SO_3)_3(PF_6)(CH_3CN)_{0.5}$ (**12**) are listed in Tables S2−S4; Eu($^5D_0$) lifetimes for $[Eu(L^{10}+H)]^{4+}$ in acetonitrile/water mixture together with calculated numbers of inner-sphere water molecules (q) are given in Table S5; Tables S7−S8 collect the axial anisotropic magnetic susceptibility parameters, contact and pseudocontact contributions, and average F_i and G_i terms calculated according to eq 13 for $[Ln(L^{10})]^{3+}$ and $[Ln(L^{10}+H)]^{4+}$ in solution; elemental analyses for the complexes are given in Table S9; molecular peaks observed by ES-MS are given in Table S10; and Eu($^5D_0$) lifetimes measured under different experimental conditions are reported in Table S11 (PDF). This material is available free of charge via the Internet at http://pubs.acs.org.

JA990898W

(64) Main, P.; Fiske, S. J.; Hull, S. E.; Lessinger, L.; Germain, D.; Declercq, J. P.; Woolfson, M. M. *MULTAN 87*; Universities of York, England, and Louvain-La-Neuve, Belgium, 1987.

(65) Hall, S. R., Stewart, J. M., Eds. *XTAL 3.2 User's Manual*; Universities of Western Australia and Maryland, 1992.